CHEMIJA
2026. Vol. 37. No. 3. P. 169–193

ISSN 0235-7216 eISSN 2424-4538
DOI: https://doi.org/10.6001/chemija.2026.37.3.1

Electrochemical study of the corrosion behaviour of steel rebar in a chloride-containing alkaline environment and the passive-film influence mechanism of Xanthium extract

Yu-chen Zhang[a],

Xiao Liu[a],

An-lan Ji[a],

Rui Ding[a*],

Yi-wen Zhang[a],

Hao-han Cao[a],

Bing Bai[a],

Xin-ting Ding[a],

Rui-qin Xu[a],

Jin-ying Li[a],

Jie Liu[b]

[a] *School of Ocean, Yantai University, Yantai, China*

[b] *School of Chemistry and Chemical Engineering, Yantai University, Yantai, China*

To develop a green corrosion inhibitor suitable for chloride-containing alkaline environments in reinforced concrete, Xanthium extract was investigated in a simulated concrete pore solution (saturated $Ca(OH)_2$ + 3.5 wt% NaCl). Open-circuit potential (OCP), electrochemical impedance spectroscopy (EIS), and potentiodynamic polarisation were employed to systematically evaluate its effect on the corrosion behaviour of carbon steel electrodes. The results show that the extract exhibits a pronounced concentration dependence. The solution containing 700 mg/L Xanthium extract shows the best performance in terms of overall impedance, Faradaic resistance, total electrode-process resistance, and long-term polarisation behaviour, followed by 1000 mg/L, whereas 200 mg/L provides the poorest overall protection. EIS analysis indicates that the extract influences steel corrosion by regulating the dielectric response of the composite film, the electrochemical reaction process, and the restricted transport process. Combined with the passive-film mechanism in alkaline media and the adsorption-film mechanism of inhibitor molecules, the effect of the extract is not simply to promote film thickening. Instead, at suitable concentrations, it stabilises the passive-film structure through surface adsorption, suppresses passive-film defect evolution, and reduces interfacial charge transfer, thereby enhancing the corrosion resistance of steel rebar in chloride-containing alkaline environments. This concentration-dependent synergy governs the final protection efficiency under the present conditions.

Keywords: natural corrosion inhibitor, Xanthium, reinforced concrete, electrochemistry

INTRODUCTION

Reinforced concrete, owing to its high mechanical strength, good construction adaptability, and relatively low engineering cost, has been widely used in port terminals, cross-sea bridges, coastal buildings, and other marine infrastructures. However, the durability of reinforced concrete is not inherently guaranteed, and its service life largely depends on whether the embedded steel rebars can remain stable over the long term. Once corrosion of the steel rebars occurs, the volumetric expansion of corrosion products will cause cracking and spalling of the concrete cover, further leading to a reduction in the cross-sectional area of the steel and a deterioration in the bond performance between steel and concrete, thereby ultimately endangering the safety and service life of the structure [1–3]. Therefore, research on the control of steel corrosion is of a great scientific significance and a considerable engineering value.

* Corresponding author. Email: dingrui@ytu.edu.cn

Under normal concrete pore-solution conditions, the high alkalinity of the system usually enables a passive film to form spontaneously on the steel surface, thus maintaining the steel in a relatively passive state [2, 4]. However, in marine environments, the long-term ingress of chlorides into concrete allows Cl^- to gradually migrate to the steel surface, significantly increasing the risk of passive-film destabilisation [1–3]. Previous studies have shown that the passive film formed on steel in alkaline environments is not an ideal dense monolayer, but rather consists of an outer deposition layer and an inner compact layer, in which the inner layer is mainly composed of Fe_3O_4 and serves as the key structure responsible for protection. During its formation, this passive film is accompanied by oxygen vacancies, iron vacancies, and interstitial Fe^{2+} defects; therefore, it is essentially a highly defective oxide film with pronounced defect characteristics. Under the continuous action of Cl^-, dissolution of film components and accumulation of interfacial defects jointly drive passive-film destabilisation, causing the film to become progressively looser, thinner, and even locally collapse [4–6]. Thus, the corrosion of steel rebar in marine environments is not simply a matter of metal dissolution, but rather the result of long-term competition between 'passivation induced by high alkalinity' and 'destabilization induced by chloride-containing media'.

To retard or suppress steel corrosion, the addition of corrosion inhibitors is an important and effective protection strategy. Corrosion inhibitors for steel rebars can improve structural durability by influencing surface reactions on the steel, regulating the state of interfacial films, and reducing the rates of anodic and cathodic reactions. Compared with some conventional inorganic or synthetic organic inhibitors, natural plant extracts have advantages such as abundant sources, renewability, environmental friendliness, and diverse molecular structures, and have therefore attracted an increasing attention in the field of metal corrosion protection in recent years [3, 7–10]. Many natural extracts are rich in phenolic hydroxyl, carboxyl, carbonyl, and aromatic conjugated structures. These functional groups not only facilitate adsorption of molecules on metal or oxide-film surfaces, but also help construct an organic protective layer with a good coverage, thereby repelling corrosion-related species such as H_2O, OH^-, Cl^-, and dissolved oxygen and weakening interfacial charge transfer and ion-transport processes [7–17].

In the strongly alkaline chloride-containing environment encountered by steel rebars, the action of natural inhibitor molecules is not unidirectionally beneficial. Molecular adsorption can further alter the formation and evolution of the passive film, and its influence is clearly dual in nature. On the one hand, the adsorbed layer may compete with H_2O and OH^- for interfacial sites, thereby hindering oxygen incorporation into oxygen vacancies and slowing the continued growth of the inner Fe_3O_4 layer, so that thickening of the passive film is constrained. On the other hand, the adsorbed layer can inhibit the dissolution and migration of lattice iron and interstitial Fe^{2+}, thereby reducing the accumulation of defects within the film and iron-atom vacancies at the metal/film interface and thus improving the integrity and stability of the film. Therefore, the final protective effect of a natural inhibitor on steel rebars does not simply depend on whether it 'promotes film thickening', but rather on the relative strength of two effects, namely 'suppressing further film growth' and 'stabilizing film structure', and this balance is strongly dependent on inhibitor concentration [4–6, 11–17].

Xanthium is a widely available natural plant resource. Previous compositional studies have shown that Xanthium extract contains a variety of phenolic acids, including chlorogenic acid, neochlorogenic acid, cryptochlorogenic acid, 1,5-dicaffeoylquinic acid, 3,5-dicaffeoylquinic acid, caffeic acid and ferulic acid, which can generally be classified into caffeoylquinic acid derivatives and small-molecule phenolic acids [18–24]. These molecules commonly possess structural features such as multiple adsorption centres, aromatic conjugated backbones, and ionisable oxygen-containing functional groups. In alkaline media, some of these functional groups may be deprotonated, thereby enhancing coordination, electrostatic attraction, and hydrogen-bonding interactions with Fe sites on the steel surface or passive-film surface. Meanwhile, the aromatic conjugated structures are also conducive to improving the adsorption stability of the molecules at the interface. It can therefore be inferred that Xanthium extract has potential as a natural corrosion inhibitor for steel rebars [11–17, 23]. However, the corrosion-inhibition behaviour of aqueous Xanthium extract in strongly alkaline chloride-containing environments and its

influence on passive films on steel rebars have not yet been systematically studied [25–27].

On this basis, Xanthium extract was selected as the research object in this work. Its influence on the corrosion behaviour of carbon steel electrodes was systematically investigated in a strongly alkaline chloride-containing simulated concrete pore solution composed of saturated $Ca(OH)_2$ and 3.5 wt% NaCl. Open-circuit potential, electrochemical impedance spectroscopy, and potentiodynamic polarisation were employed to analyse the time evolution of the interfacial state of steel rebars under different concentrations of Xanthium extract. Particular attention was paid to its influence on the dielectric process of the composite film, the electrochemical reaction process, and the overall protective performance. Its possible mechanism was further discussed in combination with the passive-film mechanism in alkaline environments and the adsorption-film mechanism of inhibitor molecules. This study is expected to provide an experimental basis for the application of Xanthium extract in the durability protection of reinforced concrete and to deepen understanding of the 'adsorption film-passive film' synergistic behaviour of natural inhibitors in strongly alkaline chloride-containing systems.

EXPERIMENTAL METHODS

Extraction of Xanthium

The fruits of Xanthium were first dried in a blast drying oven at 50–100°C and then ground into powder using a grinder. The powder was stored at room temperature. Xanthium powder and water were mixed at a mass-to-volume ratio of 10 g:100 mL and added into a three-neck flask. The mixture was heated to 95–100°C and extracted for 2 h. The extract was first centrifuged to preliminarily remove an insoluble matter. The supernatant was then further filtered under suction to remove impurities. The filtrate was placed in a blast drying oven at 50–60°C for drying. The precipitated solid was collected, ground with an agate mortar, and stored in a drying oven.

Preparation of corrosive solutions

A 0.1 mol/L NaOH solution was used as the solvent to dissolve the extracted *Xanthium* inhibitor powder. A stock solution of the natural corrosion inhibitor with a concentration of 10 g/L was thus obtained. A saturated $Ca(OH)_2$ solution was prepared to simulate the pore solution of reinforced concrete, with the solubility of $Ca(OH)_2$ being approximately 1.65 g/L. A small amount of $Ca(OH)_2$ precipitate was retained in the solution to ensure saturation. The saturated $Ca(OH)_2$ solution and the inhibitor stock solution were then mixed proportionally to prepare corrosive solutions containing different concentrations of the inhibitor. The inhibitor concentrations in the corrosive solutions were 0, 100, 200, 300, 500, 700 and 1000 mg/L, respectively. Appropriate amounts of $Ca(OH)_2$ were further added to the mixed solutions to maintain $Ca(OH)_2$ saturation. The corrosive solutions were weighed, and solid NaCl was added according to the solution mass so that the mass concentration of NaCl was 3.5 wt%. The pH value of each corrosive solution was measured with a pH meter, and a saturated NaOH solution was added dropwise to adjust the pH to 13.0–13.5.

Electrochemical measurements

Electrochemical measurements were carried out using a conventional three-electrode system, including open-circuit potential (OCP), electrochemical impedance spectroscopy (EIS), and potentiodynamic polarisation tests. A carbon steel electrode was used as the working electrode, a platinum sheet electrode as the counter electrode, and a saturated calomel electrode (SCE) as the reference electrode. For the EIS measurements, a sinusoidal potential perturbation with an amplitude of 10 mV was applied over a frequency range from 0.01 to 100000 Hz, with 10 points collected per decade. For the potentiodynamic polarisation measurements, the potential scan range was from OCP – 0.3 V to OCP + 0.5 V at a scan rate of 0.333 mV/s. The polarisation curves were fitted using the Cview software, and the EIS data were fitted using the ZimpWin software.

RESULTS AND DISCUSSION

Main components of Xanthium extract

As shown in Fig. 1, the major corrosion-inhibiting components in Xanthium extract include chlorogenic acid, neochlorogenic acid, cryptochlorogenic acid, 1,5-dicaffeoylquinic acid, 3,5-dicaffeoylquinic acid, caffeic acid and ferulic

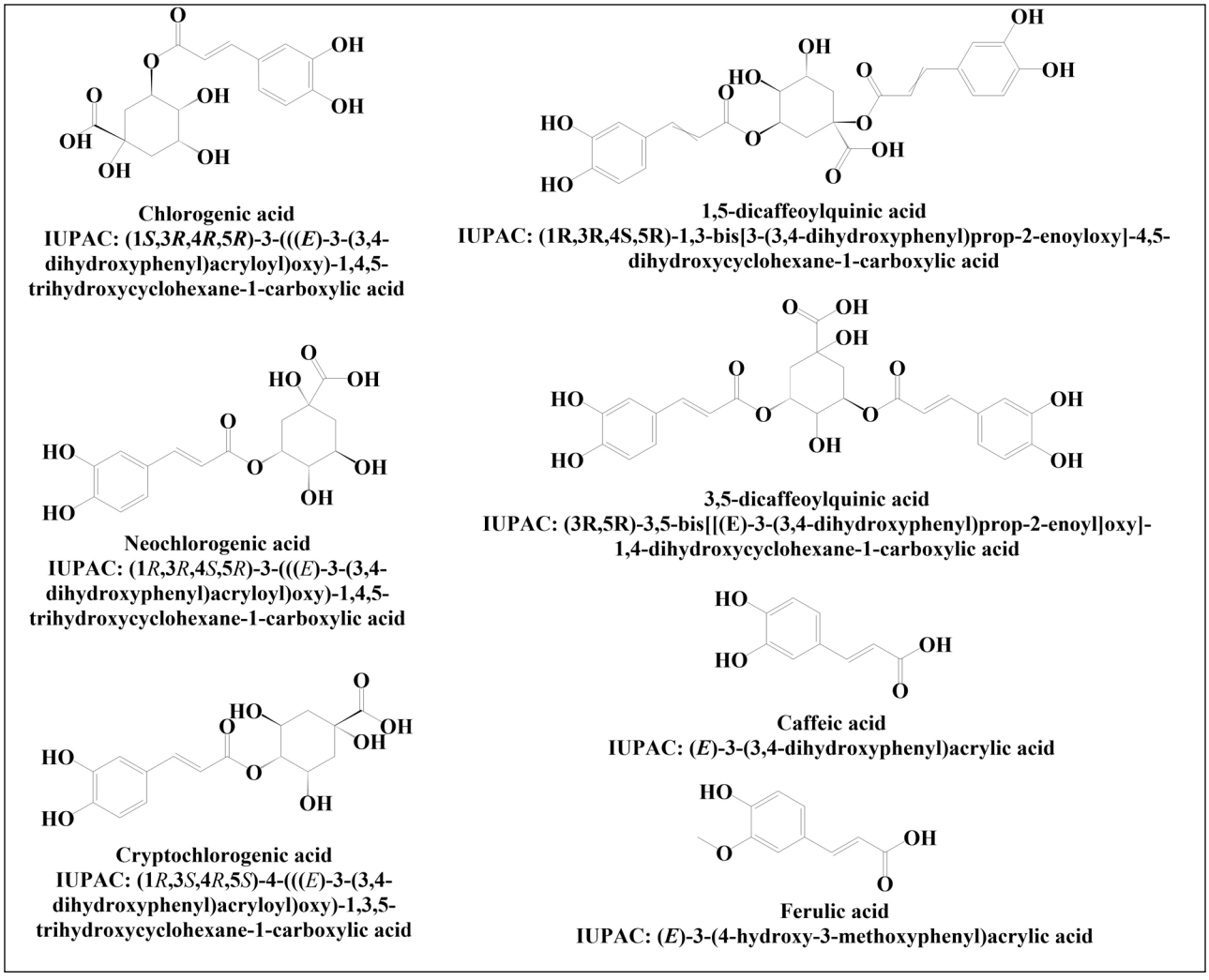

Fig. 1. Molecular structures and names of the major corrosion-inhibiting components in Xanthium extract

acid [18–24]. These compounds can generally be classified into two categories: caffeoylquinic acid derivatives and small-molecule phenolic acids. They commonly contain structural units such as aromatic rings, phenolic hydroxyl groups, carboxyl groups, ester groups, carbonyl groups, and conjugated double bonds, and therefore exhibit a relatively high polarity and a certain degree of electron delocalisation. From the molecular-structure perspective, the oxygen atoms in phenolic hydroxyl, carboxyl, and ester groups can serve as potential adsorption-active sites. In alkaline media, some functional groups may also be deprotonated, thereby enhancing coordination, electrostatic attraction, and hydrogen-bonding interactions with Fe sites on the steel surface or passive-film surface. Meanwhile, the aromatic conjugated structures facilitate electron-cloud delocalisation, which improves the adsorption stability of the molecules at the interface. Compared with smaller molecules such as caffeic acid and ferulic acid, dicaffeoylquinic acid derivatives contain more phenolic hydroxyl and carbonyl oxygen atoms and thus provide more abundant adsorption sites, making them more favourable for multipoint anchoring. In contrast, small-molecule phenolic acids may migrate and diffuse more rapidly, and may therefore more readily reach the interface and participate in adsorption at the early stage. Overall, these components share the structural characteristics of 'multiple adsorption centers, aromatic conjugated backbones, and ionizable oxygen-containing functional groups', which provide a sound molecular basis for the interfacial adsorption of Xanthium extract in strongly alkaline chloride-containing environments and for its influence on steel surface reactions and the state of the passive film.

Passive-film mechanism in alkaline environments

In strongly alkaline simulated concrete pore solutions, a passive film forms spontaneously on the surface of steel rebar. This film generally consists of an outer deposition layer and an inner compact layer. The outer layer mainly originates from the hydrolytic deposition of dissolved iron ions and may contain FeOOH and related composite products associated with environmental ions, whereas the inner layer is mainly composed of compact Fe_3O_4 and serves as the key structure determining the protective performance. In terms of the formation process, Fe atoms at the steel surface first lose electrons and undergo local structural rearrangement, entering the Fe_3O_4 lattice as lattice iron while generating oxygen vacancies in the inner layer. Subsequently, oxygen provided by H_2O or OH^- in the solution enters and occupies these vacancies, is converted into lattice oxygen, and together with lattice iron drives the continuous growth of the inner Fe_3O_4 layer [4–6, 28, 29]. Meanwhile, defects such as iron vacancies and interstitial Fe^{2+} also arise in the film, indicating that this passive film is not an ideal perfect crystal but rather a highly defective oxide film with pronounced semiconducting characteristics.

The dissolution and breakdown of the passive film do not simply involve thinning of the film layer, but are instead destabilisation processes jointly driven by dissolution of film components and accumulation of interfacial defects [4–6]. On the one hand, iron in Fe_3O_4 and Fe_2O_3 can gradually dissolve under the action of aggressive species such as Cl^-, causing the film structure to become looser. On the other hand, the dissolution of lattice iron ions from the film surface leaves iron vacancies within the film, while some Fe atoms at the steel/film interface can migrate outward in the form of interstitial Fe^{2+} and further enter the solution, thereby leaving iron-atom vacancies on the metal side. As these defects continue to form, migrate and accumulate, the integrity, adhesion and stability of the passive film progressively deteriorate, ultimately leading to thinning, collapse, or even spallation [4–6]. Therefore, whether the passive film remains stable depends not only on whether the film itself persists, but also on whether defects at the interface and within the lattice are continuously amplified.

Adsorption of molecules on the metal surface can further alter this passive-film mechanism, and its influence is distinctly dual in nature [30]. First, the adsorbed layer may compete with H_2O and OH^- for interfacial sites, thereby hindering oxygen from entering oxygen vacancies and slowing the formation of the inner Fe_3O_4 layer, so that the growth rate of the passive film decreases and the apparent film thickness becomes smaller or its thickening is restrained. Second, another effect then becomes increasingly important, namely, inhibition of the dissolution and migration of lattice iron and interstitial Fe^{2+}, which reduces the accumulation of defects within the film and iron-atom vacancies at the metal/film interface, thereby improving the integrity and protective capability of the film. Thus, adsorption does not necessarily make the passive film thicker. Under certain conditions, it may even make the film thinner; however, if it simultaneously suppresses defect evolution and film dissolution more effectively, the overall protective performance of the system can still be improved. Therefore, the final influence of adsorbed molecules on the passive film essentially depends on the relative strength of two effects, namely, 'suppressing further film thickening' and 'stabilizing film structure'. It should be particularly emphasised that this strongly depends on the concentration of the inhibitor molecules. In addition, inhibitor molecules can be anchored onto the metal surface and oxide-film surface through physical adsorption, chemical adsorption, or their synergistic combination, forming a continuous or quasi-continuous protective layer that covers active sites, repels corrosive species such as H_2O, OH^-, Cl^-, and dissolved oxygen, interrupts the interfacial contact and charge transfer required for corrosion reactions, increases the resistance to anodic metal dissolution, and suppresses cathodic oxygen reduction or hydrogen evolution, thereby reducing the corrosion current. The adsorption-inhibition performance also depends strongly on the concentration of the inhibitor molecules.

Analysis of EIS

Analysis of overall impedance level

Figure 2 shows that the variation in the Nyquist arc radius is generally consistent with that in the low-frequency impedance modulus in the Bode plots

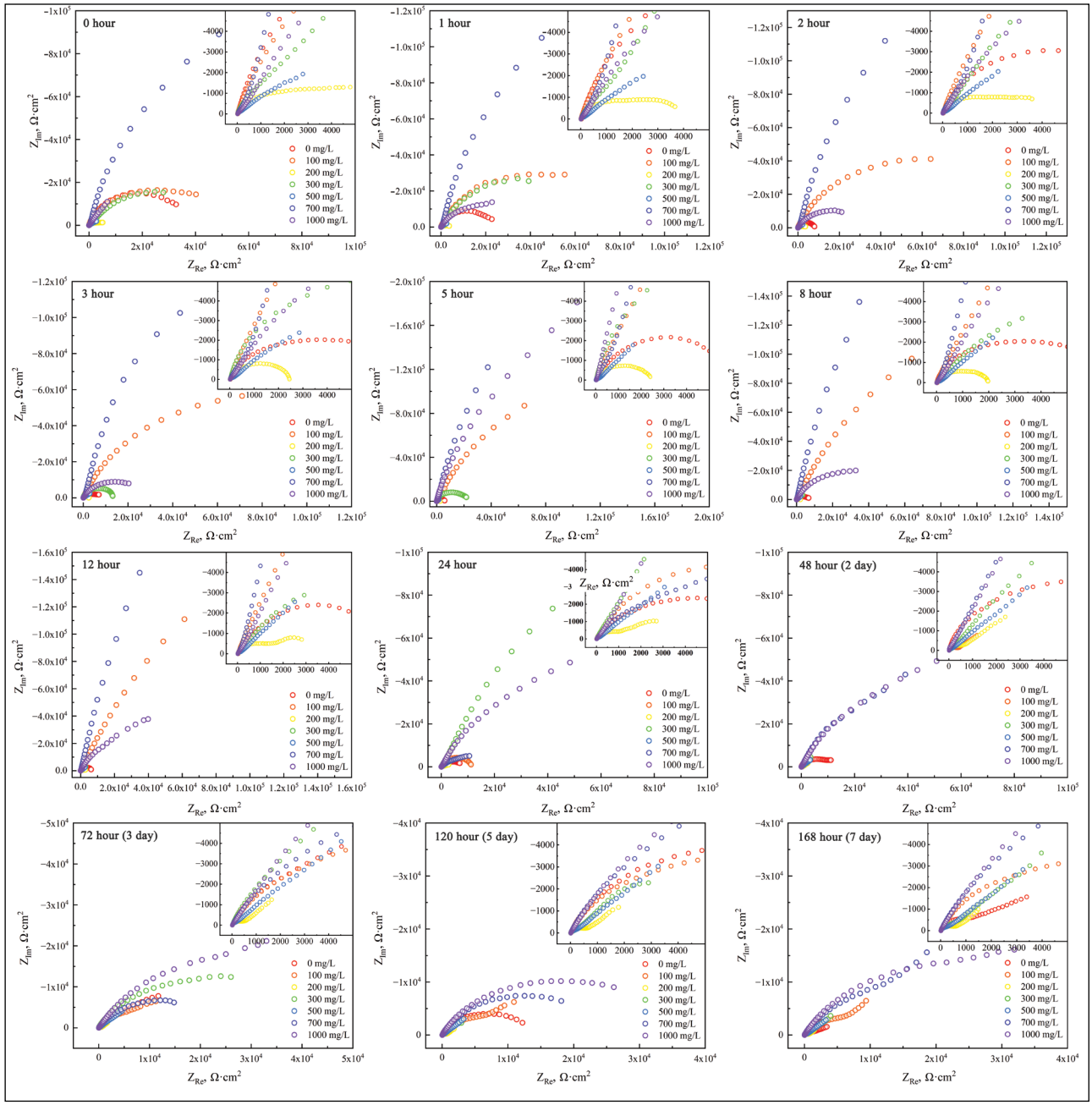

Fig. 2. Nyquist plots of electrochemical impedance spectra of carbon steel electrodes exposed for different times in 3.5 wt% NaCl + saturated $Ca(OH)_2$ solution (pH = 13.5) containing different concentrations of Xanthium extract

(Fig. 3) for systems containing different concentrations of Xanthium extract. Therefore, the low-frequency impedance modulus in Fig. 3, $|Z|_{0.01\ Hz}$, can be used as an important parameter to characterise the overall impedance level of the system and is summarised in Fig. 4a. To avoid the contingency associated with evaluating the inhibition performance based on data at only a single time point, the time-integrated average value of the low-frequency impedance modulus, $\langle|Z|\rangle_{0.01\ Hz}$, was further introduced and defined as

$$\langle |Z| \rangle_{0.01\,Hz} = \frac{1}{t}\int_0^t |Z|_{0.01\,Hz} dt, \quad (1)$$

where t is the total exposure time. This parameter shown in Fig. 4b reflects the ability of a sample at a given concentration to maintain a high interfacial impedance throughout the entire exposure period. A larger value indicates a better overall protective effect.

Considering only the impedance magnitude, the blank group already exhibited a relatively high

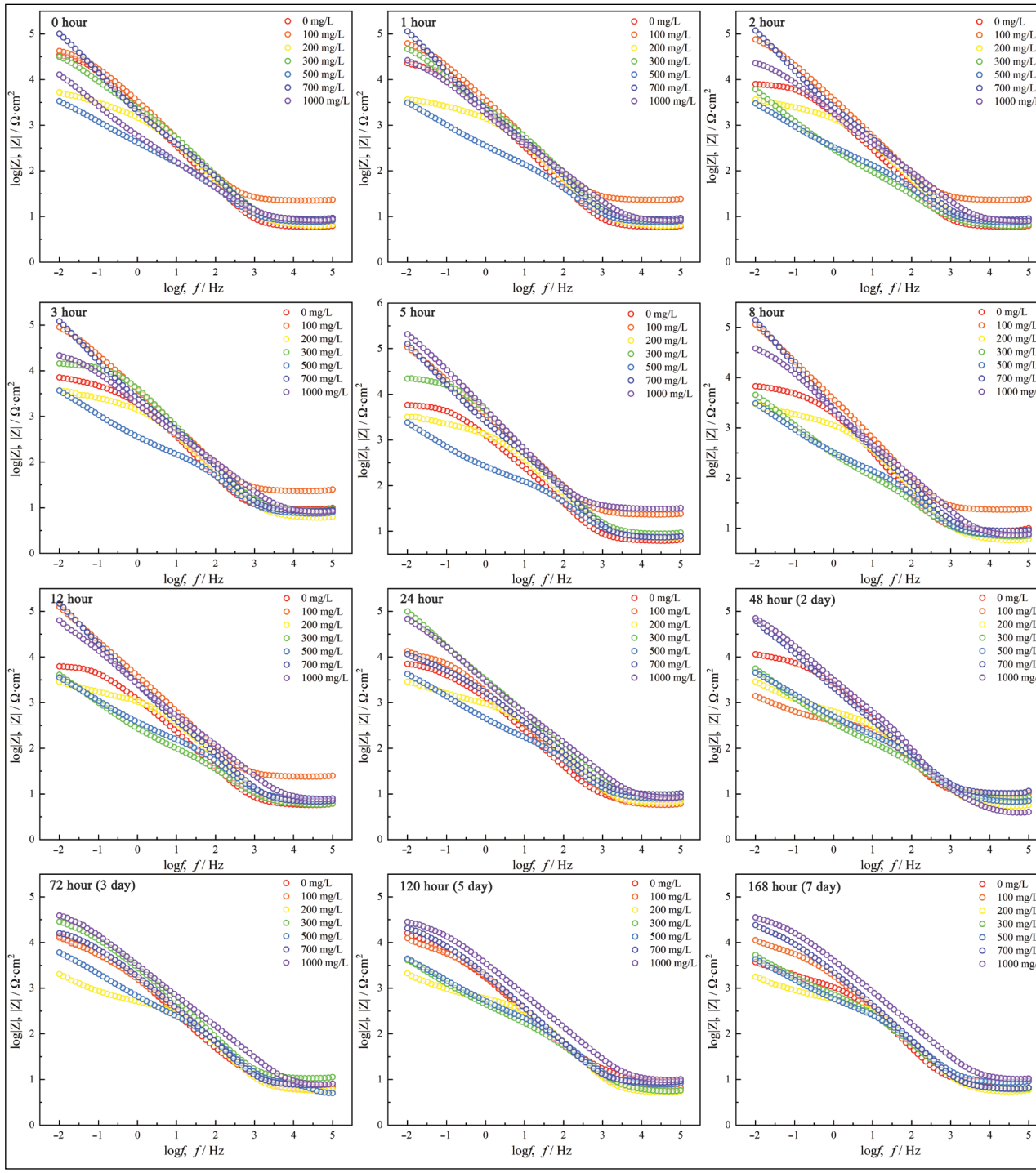

Fig. 3. Bode impedance modulus plots of the electrochemical impedance spectra of carbon steel electrodes exposed for different times in 3.5 wt% NaCl + saturated $Ca(OH)_2$ solution (pH = 13.5) containing different concentrations of Xanthium extract

impedance at 0 h, indicating that an initial passive film could be rapidly formed on the steel surface in a strongly alkaline saturated $Ca(OH)_2$ solution. Subsequently, from 2 h to 7 d, the low-frequency impedance modulus decreased markedly, indicating that although the film layer was still present under the action of Cl^-, the accumulation of defects within the film and local dissolution had already begun to weaken its protective capability. After the addition of the Xanthium inhibitor, all systems showed a clear concentration dependence. The 100 and 700 mg/L groups (the solution containing 100 or 700 mg/L Xanthium extract, in the following text, 'group' will be used as the abbreviation) exhibited a continuous increase in both the Nyquist arc radius and the low-frequency

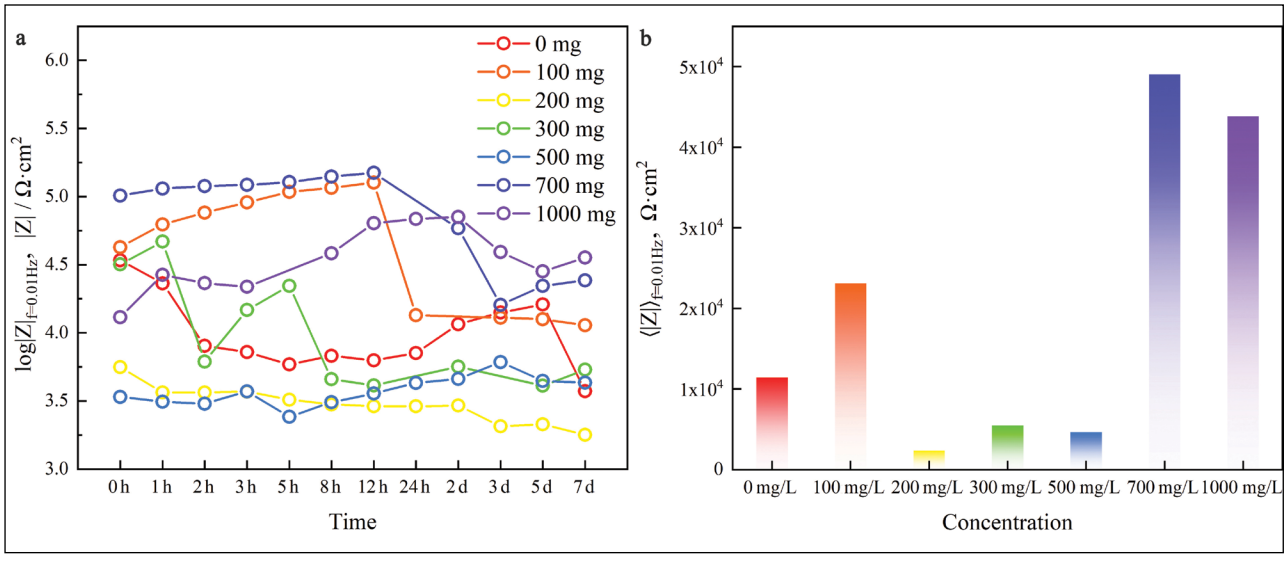

Fig. 4. (a) Low-frequency impedance modulus ($|Z|_{0.01\ Hz}$) and (b) time-integrated average low-frequency impedance modulus ($\langle|Z|\rangle_{0.01\ Hz}$) of the electrochemical impedance spectra of carbon steel electrodes exposed for different times in 3.5 wt% NaCl + saturated $Ca(OH)_2$ solution (pH = 13.5) containing different concentrations of Xanthium extract

|Z| value during 0–12 h, with 700 mg/L consistently showing the highest values and 100 mg/L the second highest, indicating that those two concentrations were the most favourable for improving the interfacial impedance at the early stage. Although the impedance of the 1000 mg/L group was lower than that of the 700 mg/L group at the initial stage, it increased steadily with time and remained at a relatively high level after 24 h. In contrast, the 200 mg/L group maintained the lowest impedance throughout the entire exposure period, while the 300 and 500 mg/L groups also showed a relatively low overall impedance, with the 300 mg/L group exhibiting more obvious fluctuations, suggesting that its interfacial state was not sufficiently stable. The $\langle|Z|\rangle_{0.01\ Hz}$ values shown in Fig. 4b further indicate that the overall protective performance followed the order: 700 mg/L > 1000 mg/L > 100 mg/L > 0 mg/L > 300 mg/L ≈ 500 mg/L > 200 mg/L.

This trend can be well correlated with the 'passive-film mechanism' and the 'adsorption-film mechanism' described in the Section 'Passive-film mechanism in alkaline environments'. The polyphenolic acid molecules in Xanthium extract contain multiple oxygen-containing active sites and aromatic conjugated structures, enabling them to adsorb on both the steel surface and the passive-film surface, cover active sites, and repel H_2O and OH^-, thereby increasing the interfacial impedance. However, in alkaline environments, adsorption exerts a dual influence. On the one hand, the adsorbed molecules compete with H_2O and OH^- for interfacial sites, thereby suppressing the continued growth of the inner Fe_3O_4 layer. On the other hand, once adsorption coverage reaches a certain level, the adsorbed molecules can inhibit the dissolution and migration of lattice iron and interstitial Fe^{2+}, slow down defect accumulation within the film, and improve film integrity. Therefore, the impedance level does not simply depend on whether film thickening is 'promoted', but rather on the relative strength of the two effects, namely, 'suppressing further film thickening' and 'stabilizing film structure'.

For the present system, the relatively low overall impedance of the 200, 300 and 500 mg/L groups indicates that, at these concentrations, the adsorbed layer had already begun to hinder the entry of OH^- and H_2O into the interface, but its coverage or compactness was still insufficient to effectively suppress passive-film defect evolution and Cl^- ingress. As a result, passive-film growth was disturbed without forming a sufficiently stable protective layer, and the overall impedance was therefore reduced. In contrast, the 100 mg/L group showed a pronounced early-stage advantage, indicating that at this lower concentration, some active molecules could rapidly reach the interface and participate in adsorption, temporarily

slowing defect accumulation without excessively suppressing passive-film formation. Consequently, the impedance increased continuously during 0–12 h. However, owing to the limited concentration, the persistence and resistance to disturbance of the adsorbed layer became insufficient at later stages, leading to a significant decrease in impedance after 24 h. The 700 mg/L group exhibited the best overall performance, indicating that at this concentration a better balance was achieved between adsorption coverage and passive-film stabilisation, so that a relatively continuous adsorbed protective layer could be formed without excessively suppressing the early passivation process. The 1000 mg/L group still maintained a very high impedance at the middle and later stages, suggesting that a stronger interfacial coverage and shielding were formed at higher concentration. However, its time-integrated average impedance was still slightly lower than that of the 700 mg/L group, indicating that an excessively high concentration may compete more strongly with OH^-/H_2O for interfacial sites at the early stage and thus restrict the establishment of the compact inner passive layer.

Based solely on impedance magnitude, the effect of the Xanthium inhibitor on steel rebar in a strongly alkaline chloride-containing environment is strongly concentration-dependent, and neither higher nor lower concentration is necessarily more favourable. The 700 mg/L group exhibited the best overall protection throughout the entire exposure period, followed by the 1000 mg/L group, which showed a greater tendency toward middle- and later-stage protection. The 100 mg/L group displayed a clear early-stage advantage, whereas the 200, 300 and 500 mg/L groups failed to establish a stable and effective synergistic protection. This indicates that the effective action of the Xanthium inhibitor essentially originates from the synergistic stabilisation between the adsorption film and the passive film, and such synergy can only be fully established within an appropriate concentration range. However, $\langle|Z|\rangle_{0.01\,Hz}$ is only a global indicator. To further distinguish the film response and the electrochemical reaction response, the fitted parameters are analysed separately in the Sections 'Analysis of the dielectric process of the film' and 'Analysis of the electrochemical reaction process'.

Fitting analysis of electrochemical impedance spectra

As shown in Figs 5 and 6, the shapes of the impedance spectra of all systems vary markedly with concentration and exposure time, but can generally be interpreted in terms of three types of responses, namely, the dielectric process of the composite film, the electrochemical reaction process, and the restricted transport process. Combined with the equivalent circuits shown in Fig. 7 and the classifications summarised in Table 1, four types of equivalent electrical circuit (EEC) were used in this study to describe the different spectral features, namely, $R_s(Q_fR_f)$, $R_s(Q_f(R_f(Q_{dl}R_{ct})))$, $R_s(Q_f(R_fW_{ec}))$ and $R_s(Q_f(R_f(Q_{dl}(R_{ct}W_s))))$. Here, R_s is the solution resistance, Q_f is the constant phase element of the composite film, R_f is the resistance of the composite film, Q_{dl} is the constant phase element of the double layer, R_{ct} is the charge-transfer resistance, W_s is the generalised finite-length Warburg diffusion element, and W_{ec} denotes the equivalent low-frequency response after coupling between the electrochemical reaction process and the restricted transport process, but without further effective separation, i.e. the combined effect of $Q_{dl}(R_{ct}W_s)$. The reason why Q rather than an ideal capacitor C was used for both the film capacitance and the double-layer capacitance is that the Nyquist arcs in this system generally exhibit depressed semicircles, while the phase-angle peaks in the Bode plots show broadening, asymmetry and dispersion in peak position, reflecting the non-ideal capacitive behaviour caused by the roughness, porosity, defect distribution, and adsorption heterogeneity of the composite film and the interface rather than an ideal homogeneous plane.

Judging from the spectral features, in the high-frequency region, all curves consistently display identifiable arcs in Fig. 5 and phase-angle peaks in Fig. 6, with peak centres roughly located in a range of 10 ~ 10^3 Hz, indicating that the dielectric process of the composite film can be stably identified in all systems. Therefore, regardless of the inhibitor concentration, Q_f and R_f must be retained as the basic elements of the equivalent circuit. This is consistent with the discussion in the Section 'Passive-film mechanism in alkaline environments' that 'the steel surface is always associated with a composite interface composed of the passive

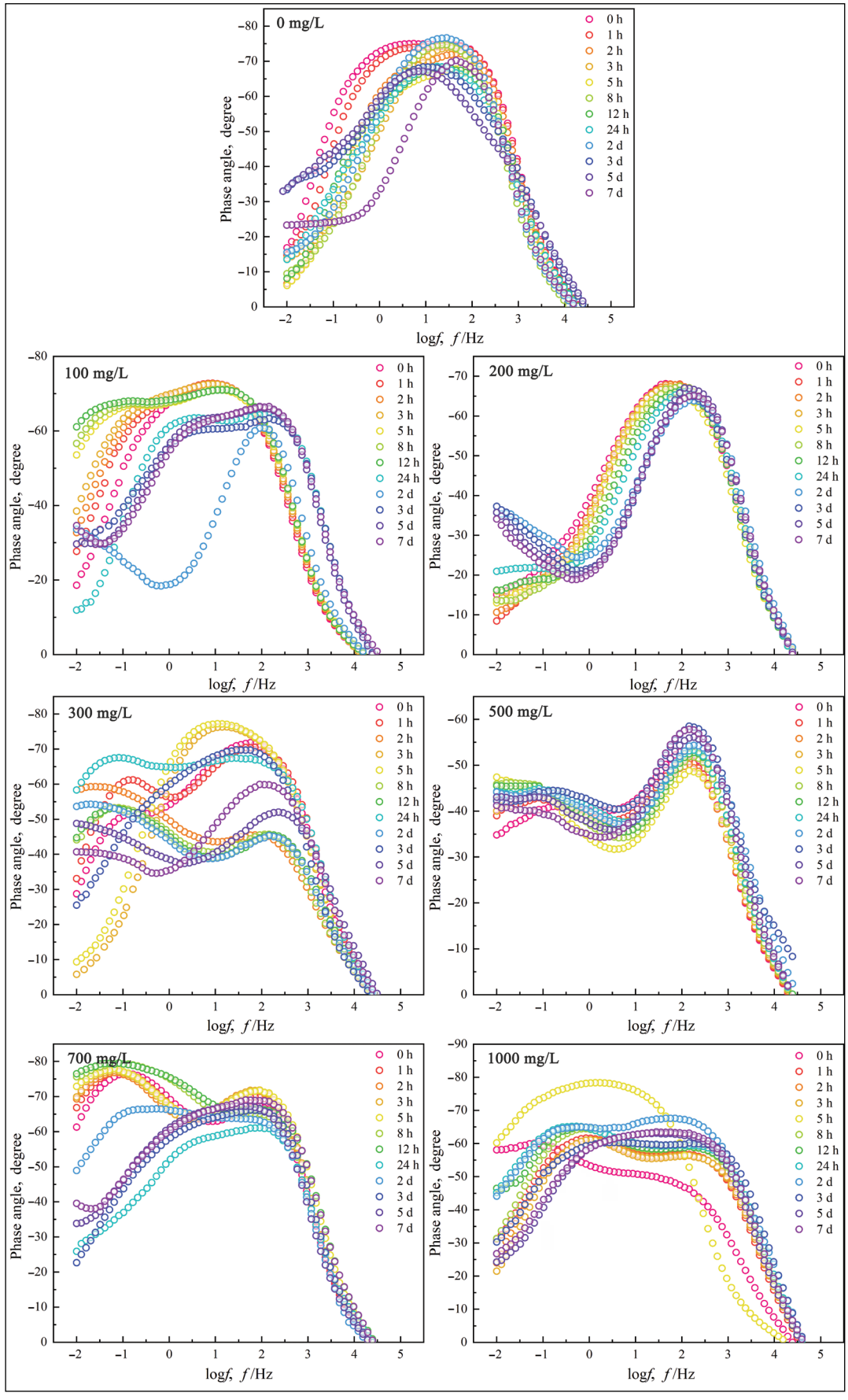

Fig. 5. Time evolution of Nyquist curves of carbon steel electrodes in 3.5 wt% NaCl + saturated $Ca(OH)_2$ solution (pH = 13.5) containing different concentrations of Xanthium extract

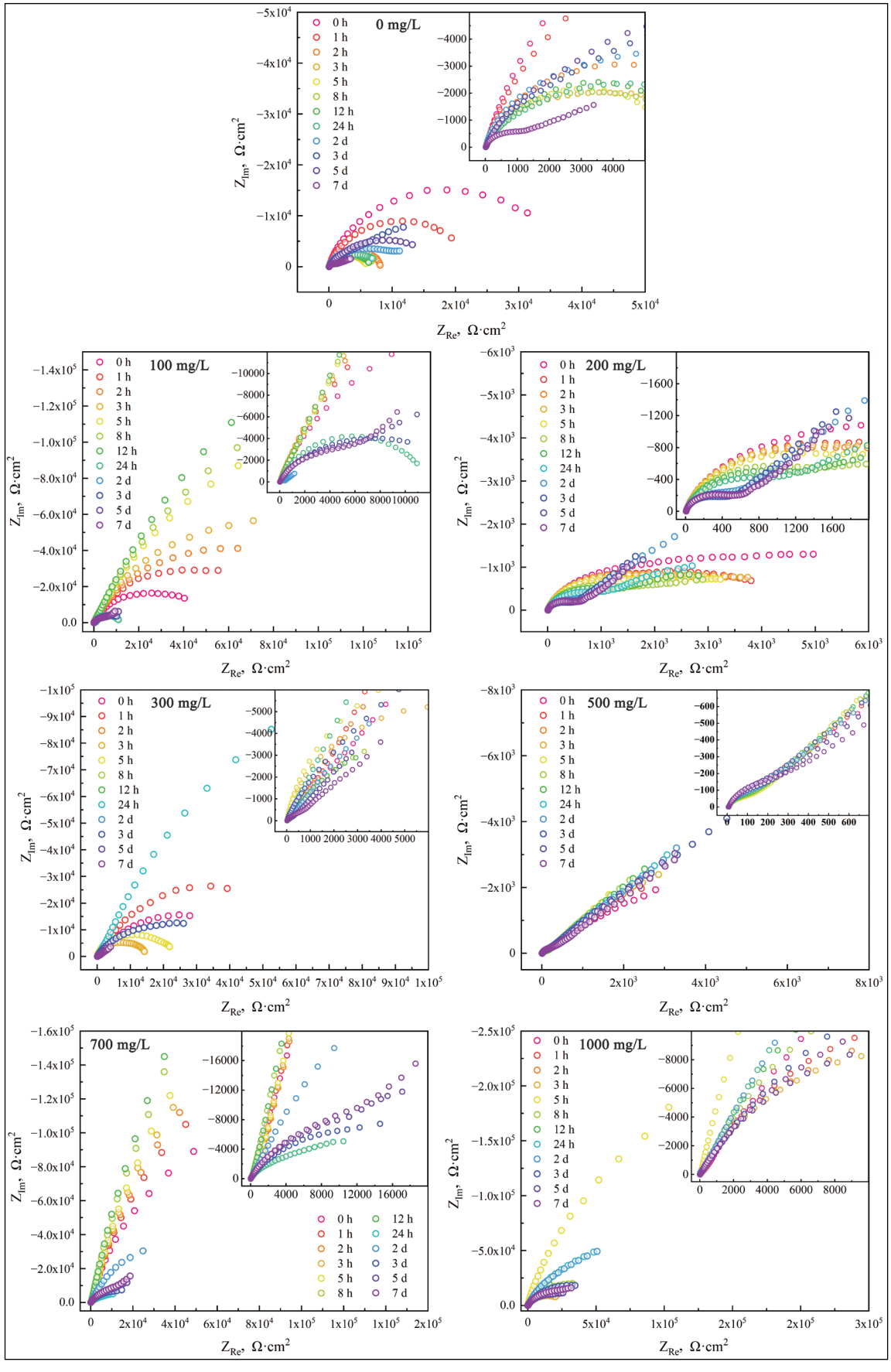

Fig. 6. Time evolution of Bode phase-angle curves of carbon steel electrodes in 3.5 wt% NaCl + saturated $Ca(OH)_2$ solution (pH = 13.5) containing different concentrations of Xanthium extract

film and the adsorbed layer'. Because molecules from the Xanthium extract can adsorb on both the steel surface and the oxide-film surface, while the steel itself forms a passive film in the strongly alkaline environment, the high-frequency response measured by EIS does not arise solely from the adsorption film or the passive film alone, but is more appropriately described as the dielectric process of a corrosion-inhibition/passivation composite film.

For the 0, 100, 300, 700 and 1000 mg/L systems, the circuit $R_s(Q_f(R_f(Q_{dl}R_{ct})))$ was used for fitting, as listed in the Table. Their common feature is that, in addition to the high-frequency peak, a second time constant associated with the electrochemical reaction process can still be identified in the low-frequency region. Although in many cases these two peaks in Fig. 6 are not completely separated, but rather appear as broadened merged peaks, a main peak with a shoulder, or a pronounced tail on the low-frequency side, the two-level arc features in the Nyquist plots (Fig. 5) still allow the dielectric process of the composite film and the interfacial charge-transfer process to be simultaneously identified. For the blank group (0 mg/L), the phase-angle curves are mostly characterised by broad asymmetric peaks, and the low-frequency region of the Nyquist plots shows curved arcs rather than linear tails, indicating that although a passive film forms in the absence of an inhibitor, the interfacial reaction process remains identifiable under the action of chloride ions. The 100 mg/L system exhibits more pronounced double peaks or shoulder peaks at most times, indicating that the low-concentration extract participates in interfacial adsorption, but does not eliminate the low-frequency reaction process. The 300 mg/L system shows more complex variations in peak shape, and the degree of separation between the two time constants fluctuates with time, suggesting that the adsorbed layer and the passive film undergo continuous rearrangement at this concentration. By contrast, the 700 and 1000 mg/L systems maintain clear high-frequency film responses and identifiable low-frequency reaction responses over relatively long exposure periods, without developing stable diffusion tails. This indicates that at relatively high concentrations, a stronger synergy is established between the adsorption film and the passive film. Although charge transfer still exists at the interface, the film layer can more effectively suppress pore transport and continuous amplification of defects. This is also consistent with the higher overall impedance levels of the 700 and 1000 mg/L groups described in the Section 'Analysis of overall impedance level'.

The circuit selection for the 200 mg/L system is distinctly different. According to the Table, $R_s(Q_fR_f)$ was used from 0 h to 1 d, while $R_s(Q_f(R_fW_{cc}))$ was used from 2 to 7 d. As can be seen from Figs 5 and 6, at the early stage, this system exhibits only a pronounced film response in the high-frequency region, whereas in the low-frequency region there is neither a clearly separated second arc nor a stably identifiable low-frequency phase-angle peak. Therefore, only the dielectric process of the composite film can be extracted as a significant response. It should be noted that this does not mean that no electrochemical reaction exists at the interface, but rather that its response cannot be effectively separated spectrally from the film process. At the middle and later stages, the low-frequency end of the Nyquist plots begins to show a nearly linear tail, while the low-frequency end of the phase-angle curves shows a reduced downward trend, local upturn, or half-peak feature, indicating the emergence of restricted transport behaviour in the system. However, the time constants of this transport feature and the charge-transfer process are very close, and the two are coupled at the apparent level, making it difficult to separate Q_{dl} and R_{ct} stably. Therefore, describing the low-frequency response with W_{ec} is more reasonable. Here, $(Q_{dl}R_{ct})$ is not merged with (Q_fR_f); instead, $Q_{dl}(R_{ct}W_s)$ is equivalently represented by W_{ec}. The reason is that the high-frequency film phase-angle peak remains clearly identifiable and its physical assignment is explicit, whereas what cannot be resolved is the coupled part of the interfacial reaction and restricted transport on the low-frequency side of the film peak. Thus, the unresolved complexity should be retained at the low-frequency end rather than being projected backward to obscure the already well-identified film process. This result indicates that at 200 mg/L, the adsorbed layer fails to establish a stable and effective dual-time-constant structure and, at later stages, induces coupled restricted transport associated with pore transport, ion migration within the film, and defect evolution, which is consistent with its lowest overall impedance and poorest overall protective performance.

The 500 mg/L system shows a clear transition from 'no diffusion' to 'with diffusion'. As listed in the Table, $R_s(Q_f(R_f(Q_{dl}R_{ct})))$ was used from 0 to 3 h,

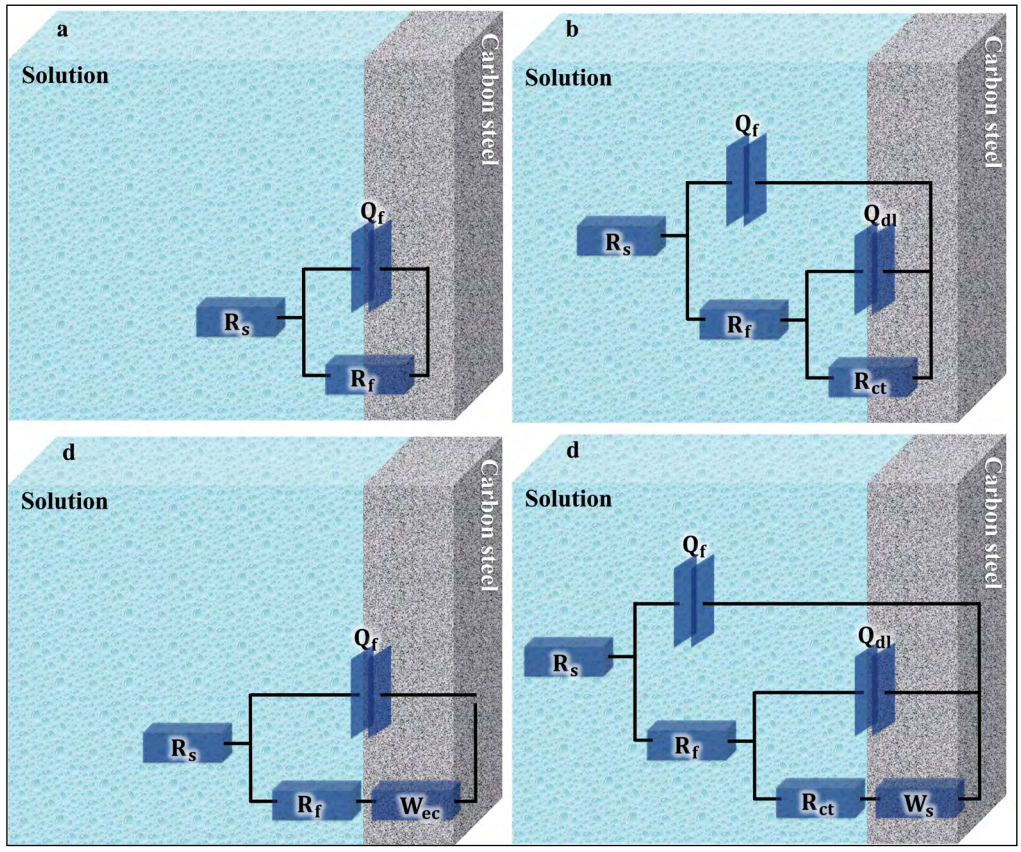

Fig. 7. Equivalent circuits used for fitting the electrochemical impedance spectra

while $R_s(Q_f(R_f(Q_{dl}(R_{ct}W_s))))$ was used from 5 h to 7 d. At the early stage, both high-frequency film responses and low-frequency reaction responses can still be identified in Fig. 5, and the low-frequency end of the Nyquist plots is dominated by curved arcs; therefore, a dual-time-constant circuit is sufficient. After 5 h, the low-frequency end of the Nyquist plots gradually develops into a distinct near-linear tail, accompanied by a slight curvature at even lower frequencies. Meanwhile, in addition to the high-frequency peak, the phase-angle curves exhibit an upturn followed by a decline at the low-frequency end. These spectral features are more consistent with the theoretical characteristics of the finite-length diffusion element W_s shown in Fig. 8 than with those of the ideal semi-infinite Warburg element W. The ideal W corresponds to an infinitely thick diffusion layer, for which the Nyquist plot should remain close to a 45° straight line over a broad range and the impedance should approach infinity as $f \rightarrow 0$. In contrast, the low-frequency tail observed in the present study does not remain at 45°, and instead shows convergence and curvature in the very low-frequency region, which is more consistent with a restricted diffusion along a finite-thickness transport path. Therefore, using W_s is more appropriate than using W. Its physical meaning should not be narrowly interpreted as diffusion of species in the solution, but more broadly as the combined manifestation of ion migration in the pores of the composite film, defect-related transport, and restricted interfacial transport. The appearance of W_s in the 500 mg/L system at the middle and later stages indicates that although the film process and charge-transfer process are still identifiable at this concentration, the interface has already developed significant transport limitations. This suggests that the adsorbed layer does not form the stable synergistic protection seen at 700 and 1000 mg/L, but instead retains defect channels or non-uniform transport pathways through which aggressive species can penetrate.

The selection of equivalent circuits in Fig. 7 was therefore not based solely on the goodness of fit, but first on the physical assignment inferred from the number of Nyquist arcs, the morphology of the low-frequency tail, and the number, symmetry, shoulder characteristics, and low-frequency trends of the Bode phase-angle peaks. In general, the 0, 100,

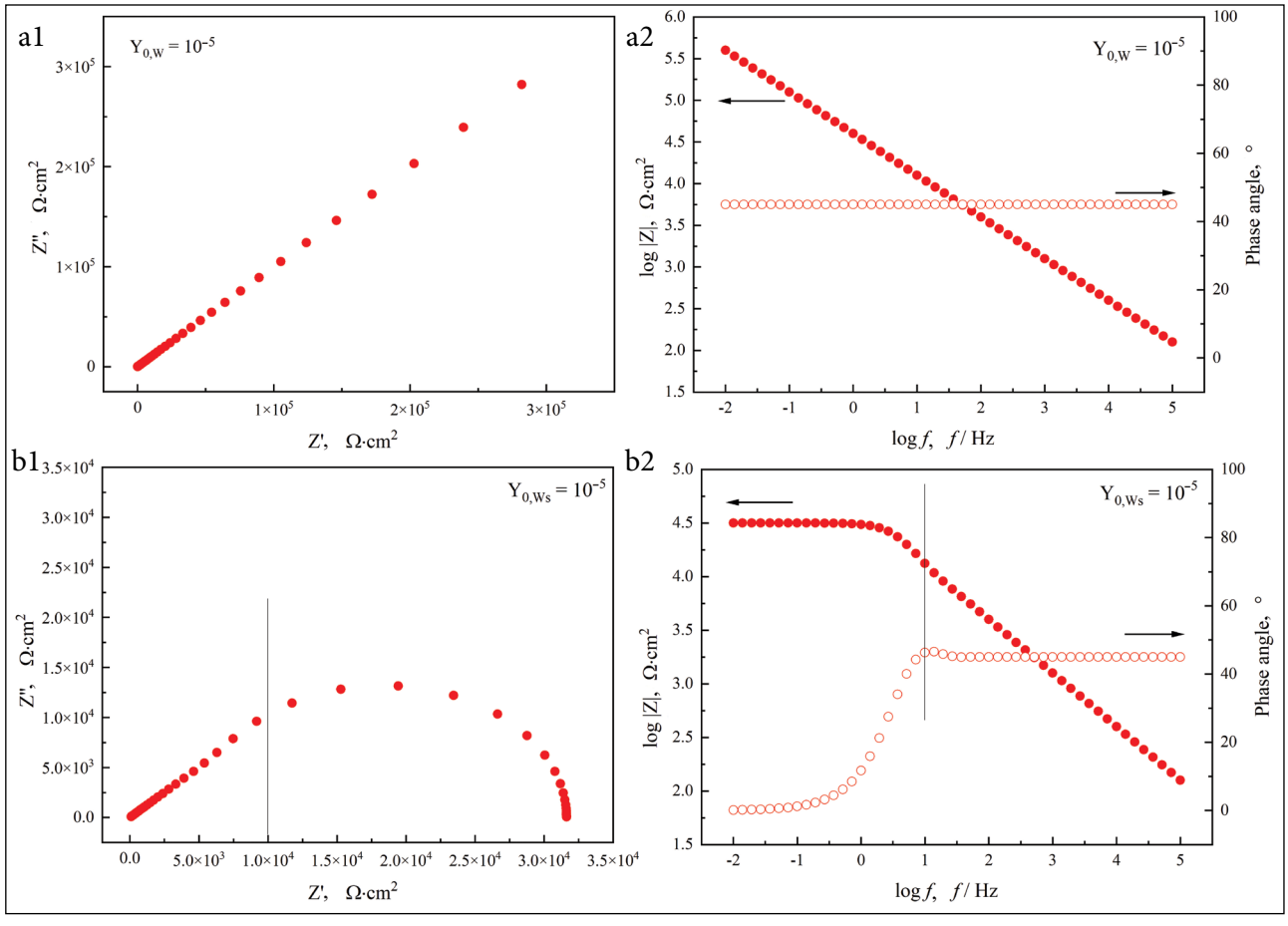

Fig. 8. Theoretical impedance spectra of (a) the semi-infinite diffusion element *W* and (b) the finite-length diffusion element W_s: (a1, b1) Nyquist plots; (a2, b2) Bode plots

300, 700 and 1000 mg/L systems are dominated by a 'composite-film dielectric process + electrochemical reaction process' framework; the 200 mg/L system evolves from a state in which 'only the film process can be identified' to one in which 'low-frequency electrochemical reaction-transport coupling dominates'; and the 500 mg/L system belongs to a dual-time-constant system at the early stage but develops a distinct finite-length restricted transport feature at the middle and later stages. These results indicate that the effect of the Xanthium inhibitor on steel rebar in a strongly alkaline chloride-containing environment is essentially achieved by altering the synergistic state between the adsorbed layer and the passive film, thereby influencing the degree of separation and dominance of the film process, interfacial reaction process, and defect-related transport process. The superior overall impedance of the 700

Table. **Summary of the equivalent circuits used for fitting the electrochemical impedance spectra**

Concentration, mg/L	Time											
	0 h	1h	2h	3 h	5 h	8 h	12 h	1 d	2 d	3 d	5 d	7 d
0	$R_s(Q_f(R_f(Q_{dl}R_{ct})))$											
100	$R_s(Q_f(R_f(Q_{dl}R_{ct})))$											
200	$R_s(Q_fR_f)$								$R_s(Q_f(R_fW_{ec}))$			
300	$R_s(Q_f(R_f(Q_{dl}R_{ct})))$											
500	$R_s(Q_f(R_f(Q_{dl}R_{ct})))$				$R_s(Q_f(R_f(Q_{dl}(R_{ct}W_s)))$							
700	$R_s(Q_f(R_f(Q_{dl}R_{ct})))$											
1000	$R_s(Q_f(R_f(Q_{dl}R_{ct})))$											

and 1000 mg/L systems arises precisely because they remain mainly within the two-process framework of 'film + reaction' without developing pronounced diffusion control, whereas the poorer performance of the 200 and 500 mg/L systems is closely related to their greater tendency to induce low-frequency coupling or restricted transport features.

Analysis of the dielectric process of the film

Based on the fitted EEC, the complete fitted parameters are summarised in the Table. Figure 9 presents the equivalent capacitance C_f of the constant phase element Q_f for the composite film and its time-integrated average value $\langle C_f \rangle$, as well as the film resistance R_f and its time-integrated average value $\langle R_f \rangle$. For a constant phase element Q, the equivalent capacitance is calculated as

$$C = (Y_0)^{1/n}(R_{||})^{(1-n)/n}, \quad (2)$$

where Y_0 is the admittance coefficient of the constant phase element, n is the dispersion exponent characterising the deviation from an ideal capacitive behaviour, and $R_{||}$ is the resistance connected in parallel with Q. For the film process, $R_{||} = R_f$.

The value of C_f cannot be interpreted in isolation simply as 'the larger, the better' or 'the smaller, the better'. According to the parallel-plate capacitance relation,

$$C = \varepsilon S/d, \quad (3)$$

an increase in C_f may indicate a larger effective film area, a thinner film, or the presence of hydrated phases and loose components with a higher

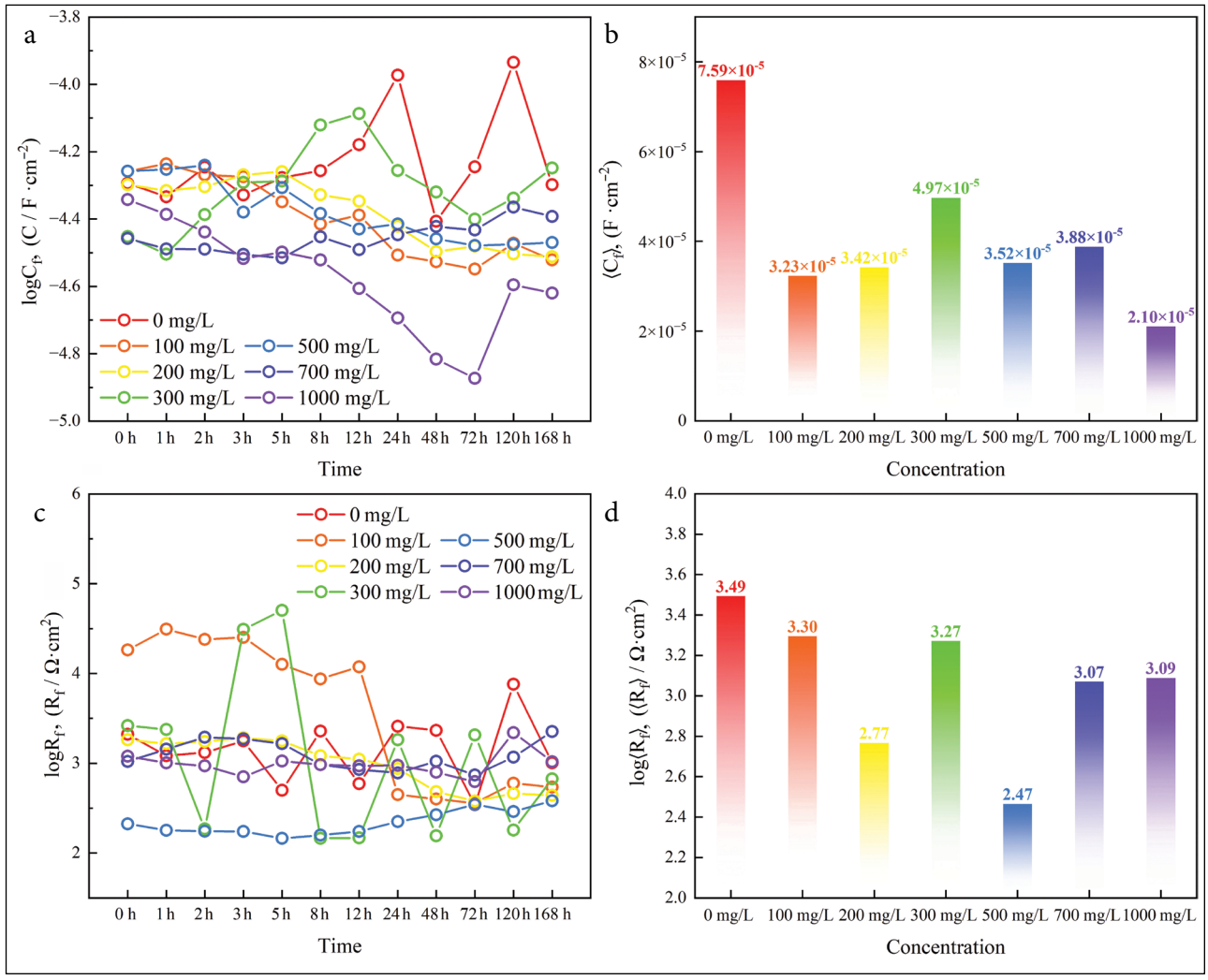

Fig. 9. (a) Equivalent capacitance of the composite film, C_f, and (b) its time-integrated average value $\langle C_f \rangle$, and (c) resistance, R_f, and its time-integrated average value $\langle R_f \rangle$, for carbon steel electrodes exposed for different times in 3.5 wt% NaCl + saturated $Ca(OH)_2$ solution (pH = 13.5) containing different concentrations of Xanthium extract

dielectric constant in the film. Conversely, a decrease in C_f may result from thickening of the film, a decrease in an effective coverage area, or a reduction in the dielectric constant of the composite film caused by the participation of the organic adsorbed layer. Therefore, C_f must be evaluated together with R_f, and in conjunction with the overall impedance and spectral features discussed above.

As shown in Fig. 9(a, b), the blank group has the highest $\langle C_f \rangle$, reaching 7.59×10^{-5} F·cm^{-2}; the 300 mg/L group ranks second, with 4.97×10^{-5} F·cm^{-2}; the value for 700 mg/L is 3.88×10^{-5} F·cm^{-2}; those for 500 and 200 mg/L are 3.52×10^{-5} and 3.42×10^{-5} F·cm^{-2}, respectively; the 100 mg/L group is slightly lower, at 3.23×10^{-5} F·cm^{-2}; and the 1000 mg/L group has the lowest value, 2.10×10^{-5} F·cm^{-2}. The blank group shows a relatively high C_f, while Fig. 9(c, d) indicate that its $\langle R_f \rangle$ is also highest, suggesting that in the absence of an inhibitor, the strongly alkaline environment does indeed drive the rapid formation and continuous evolution of a passive film on the steel surface. However, this combination of 'high C_f + high R_f' does not imply the best protection, because the overall impedance of the blank group was shown above not to be highest. Rather, this indicates that the blank system forms a continuously growing but not fully stable composite film, which possesses a certain thickness and barrier property, but is also associated with a relatively large effective interfacial area, stronger hydration characteristics, or more defects and outer-layer deposits. As a result, the film-related parameters are large, whereas the overall protective capability remains limited by defect accumulation.

For the 100 mg/L system, R_f is clearly higher during 0–12 h, but decreases significantly after 24 h (Fig. 9c), whereas C_f decreases gradually overall (Fig. 9a). This indicates that at low concentration, Xanthium extract molecules can rapidly participate in interfacial adsorption at the early stage and act synergistically with the natural passivation process to increase the film resistance. However, as exposure proceeds, the persistence of the adsorbed layer at this concentration becomes insufficient and the film-stabilising effect weakens, resulting in a later decline in R_f.

As shown in Fig. 9(a, b), the 200 mg/L system is characterised by an overall relatively low C_f, a relatively low R_f, and only a mild variation with time (Fig. 9c, d). Meanwhile, its $\langle C_f \rangle$ is 3.42×10^{-5} F·cm^{-2}, and log $\langle R_f \rangle$ = 2.77, both of which are clearly lower than those of the blank, 100, 300, 700 and 1000 mg/L groups, and are only higher than those of the 500 mg/L group. Combined with the W_{ec}-coupling feature appearing at the middle and later stages and its lowest overall impedance described above, it can be inferred that this concentration neither promotes the formation of a stable composite film with a high barrier performance nor effectively suppresses defect evolution within the film.

The most prominent characteristic of the 300 mg/L system is its strong fluctuation. Its C_f increases markedly at 8–12 h (Fig. 9a), while R_f exhibits large variations at 2, 8–12, and after 48 h (Fig. 9c), indicating a pronounced competition and rearrangement between the adsorbed layer and the passive film at this concentration. On the one hand, the adsorbed molecules may cover the interface intermittently, thereby changing the dielectric constant and effective area of the film. On the other hand, they also compete with OH^- and H_2O for interfacial sites, rendering the continued growth and defect repair of the passive film unstable. Therefore, the 300 mg/L system does not form a continuously uniform protective film, but more closely resembles a continuously reconstructed composite interface, which is consistent with its relatively low overall impedance and strong temporal fluctuation.

The distinction between 500 and 700/1000 mg/L is particularly important. Although C_f for the 500 mg/L system is not high, its $\langle R_f \rangle$ is lowest (Fig. 9d), indicating that a 'low C_f' in this case does not correspond to a better film barrier performance. Combined with the finite-length restricted transport feature W_s appearing after 5 h, a more reasonable interpretation is that the film formed at this concentration is not compact, and pore transport and ion migration within the film remain pronounced. Consequently, R_f is low and diffusion control emerges at the low-frequency end. By contrast, although the R_f values of the 700 and 1000 mg/L systems are only at an intermediate level, both show lower and more stable C_f values, especially the 1000 mg/L system, which has the lowest C_f. This suggests that at relatively high concentrations, the inhibitor is more likely to form an organic-rich composite film with a more continuous coverage and a lower dielectric constant, thereby restricting the development of hydrated phases and defect channels. The 700 mg/L system shows a better balance, namely, a not-high C_f, a stable R_f, and no

obvious diffusion feature, which is consistent with its best overall impedance performance in the Section 'Analysis of overall impedance level'.

The analysis of the dielectric process of the film indicates that the effect of the Xanthium inhibitor on the composite film on the steel surface is not simply to 'make the film thicker' or 'increase the resistance,' but rather to jointly determine the variations in C_f and R_f by regulating the film thickness, an effective coverage area, the dielectric composition, and defect evolution. The blank group tends to form a continuously growing but defect-rich passive film. The 100 mg/L system shows a distinct early-stage resistance-increasing effect but an insufficient long-term stability. The 200 and 300 mg/L systems fail to establish a stable and uniform protective film. The 500 mg/L system forms a film with a poor barrier performance and an accompanying restricted transport. The 700 and 1000 mg/L systems are more favourable for obtaining a corrosion-inhibition/passivation composite film with a more stable structure and fewer defects, among which 700 mg/L shows the best overall performance.

Analysis of the electrochemical reaction process

Figure 10 presents the Faradaic resistance R_{fa} and its time-integrated average value $\langle R_{fa} \rangle$, as well as the total electrode-process resistance R_{total} and its time-integrated average value $\langle R_{total} \rangle$. Here, R_{fa} is used to characterise the degree to which the interfacial

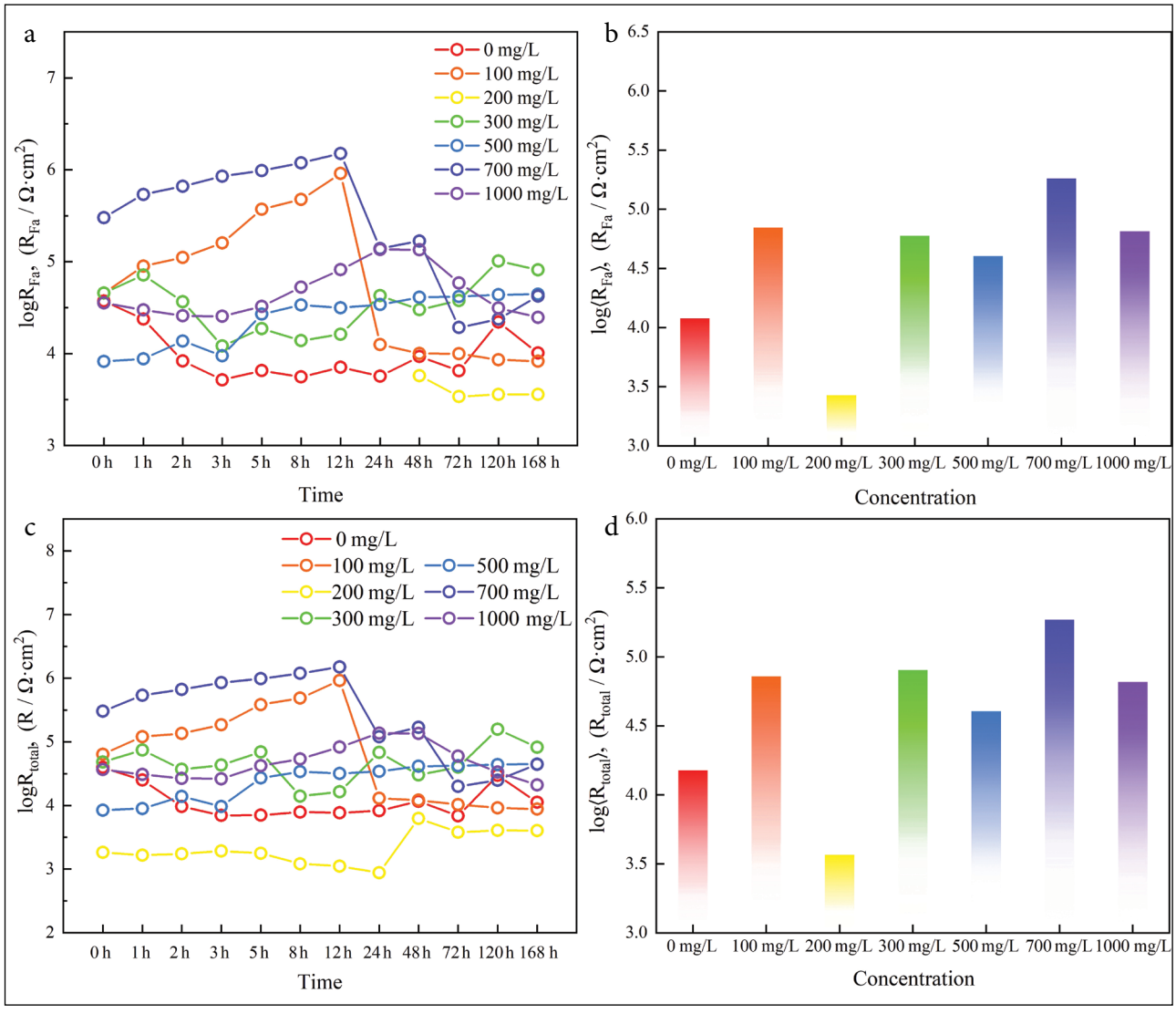

Fig. 10. (a) Faradaic resistance R_{fa} and (b) its time-integrated average value $\langle R_{fa} \rangle$, and (c) total electrode-process resistance R_{total} and its time-integrated average value $\langle R_{total} \rangle$, of carbon steel electrodes exposed for different times in 3.5 wt% NaCl + saturated $Ca(OH)_2$ solution (pH = 13.5) containing different concentrations of Xanthium extract

Faradaic process is inhibited; in essence, it reflects the hindrance imposed on charge transfer across the interface by anodic metal dissolution, the coupled cathodic reaction, and defect-related transport. $R_{total} = R_f + R_{fa}$, in turn, represents the total resistance obtained by superimposing the Faradaic-process resistance on the barrier effect of the film, and can therefore more comprehensively reflect the overall resistance of the electrode to actual corrosion reactions. For different equivalent circuits, the calculation of R_{fa} differs. When the system contains only the $Q_{dl}R_{ct}$ branch, $R_{fa} = R_{ct}$; when finite-length restricted transport W_s appears at low frequencies, $R_{fa} = R_{ct} + R_{W_s}$; and when the low-frequency electrochemical reaction and restricted transport are coupled and can only be represented by W_{ec}, $R_{fa} + R_{W_{ec}}$. This treatment is consistent with the equivalent circuits adopted for different concentration systems in Fig. 7 and the Table.

As shown in Fig. 10a, the 200 mg/L group consistently exhibits the lowest R_{fa}, with a time-integrated average value of only about $10^{3.4}\Omega \cdot cm^2$, whereas the 700 mg/L group gives the highest value, with log $\langle R_{fa} \rangle$ of approximately 5.25; the 100, 300, 500 and 1000 mg/L groups fall in between (Fig. 10b). In terms of time evolution, R_{fa} for the 700 mg/L group increases continuously during 0–12 h, indicating that the interfacial Faradaic reaction is most strongly suppressed at the early stage at this concentration. The 100 mg/L group also shows a clear increase during the first 12 h, but then decreases rapidly after 24 h. The 1000 mg/L group remains relatively stable overall and stays at an intermediate-to-high level. The 300 mg/L group fluctuates considerably, the 500 mg/L group is relatively stable but remains at an intermediate level overall, and the 200 mg/L group stays low throughout the entire period. As discussed in the Section 'Passive-film mechanism in alkaline environments', although steel rebar can form a passive film spontaneously in a strongly alkaline environment, Cl^- promotes dissolution of film components, generation of defects, and outward migration of interstitial Fe^{2+}, thereby weakening the interfacial reaction resistance. If the adsorbed molecules can effectively cover active sites and suppress the dissolution and migration of lattice iron and interstitial Fe^{2+}, R_{fa} will increase. Therefore, the significantly higher R_{fa} of the 700 mg/L group indicates that this concentration is most effective in suppressing defect-driven Faradaic reactions, whereas the 200 mg/L group indicates that its adsorbed layer neither effectively stabilises the passive film nor blocks the interfacial reaction pathways.

The R_{total} values shown in Fig. 10c, d follow trends generally similar to those of R_{fa}, but because they also include the contribution of R_f, they are more sensitive to the barrier effect of the composite film. The 700 mg/L group again exhibits the highest log $\langle R_{total} \rangle$, about 5.30 (Fig. 10d), indicating that not only is the Faradaic reaction process suppressed, but also that the film process does not noticeably compromise the overall protection, thus reflecting the best synergistic protection. The 100, 300 and 1000 mg/L groups form the second tier. Among them, the log $\langle R_{total} \rangle$ of the 300 mg/L group is slightly higher than its log $\langle R_{fa} \rangle$, suggesting that although the Faradaic process fluctuates considerably in this group, the film barrier still provides a certain compensating effect. The 1000 mg/L group remains relatively stable overall, indicating that its adsorbed layer is more continuous and suppresses both interfacial reactions and film defects, although less effectively than the 700 mg/L group. The $\langle R_{total} \rangle$ of the 500 mg/L group is clearly lower than those of the 100, 300, 700 and 1000 mg/L groups, which is fully consistent with its lower R_f and the restricted-transport feature W_s appearing at the middle and later stages. This indicates that although some reaction resistance exists at this concentration, pore migration within the film and defect-related transport remain significant, thereby limiting the overall protection level. The 200 mg/L group remains lowest, indicating that neither the film process nor the Faradaic process establishes an effective barrier.

It should be noted that the ranking of R_{fa} and R_{total} does not necessarily coincide exactly with the ranking of the overall impedance based on $|Z|_{0.01\ Hz}$ in the Section 'Analysis of overall impedance level'. This is because the low-frequency impedance modulus is influenced not only by resistance, but also by non-ideal capacitance, time-constant distribution, and the degree of process coupling. By contrast, R_{fa} and R_{total} correspond more directly to the two questions of 'how difficult it is for the interfacial reaction to occur' and 'how difficult it is, overall, for charge to pass through the film plus reaction pathway'. Therefore, although the 300 mg/L group attains a relatively high $\langle R_{total} \rangle$, its previously observed strong fluctuations, obvious variations in film parameters, and an unremarkable overall low-frequency impedance

indicate that this concentration is better described as showing 'local stage-wise resistance enhancement' rather than 'stable protection throughout the entire period'. The same is true of the 100 mg/L group: its R_{fa} and log R_{total} are relatively high at the early stage, but decline significantly at later stages. In contrast, the 700 mg/L group combines a high R_{fa}, a high R_{total}, and a high overall impedance, indicating that it achieves the best balance among the suppression of interfacial charge transfer, the reduction of defect evolution, and the maintenance of the stability of the composite film. The 1000 mg/L group ranks second, tending more toward a relatively stable but slightly milder sustained protection.

The analysis of the electrochemical reaction process indicates that the Xanthium inhibitor does not function simply by increasing film thickness, but rather by regulating the synergistic relationship between the adsorbed layer and the passive film, thereby altering the interfacial Faradaic reaction resistance and the combined film-plus-reaction resistance. The 700 mg/L group exhibits the highest R_{fa} and R_{total}, indicating that it is most effective in suppressing the actual corrosion reaction of steel rebar in a strongly alkaline chloride-containing environment. The 1000 and 100 mg/L groups rank next, although the former is more stable and the latter shows a stronger early-stage advantage. The 300 mg/L group has a certain total resistance, but an insufficient stability. The 500 mg/L group is limited by weak film barrier properties and restricted-transport characteristics. The 200 mg/L group shows the worst overall performance. These results are fully consistent with the evidence obtained above from the overall impedance, spectral fitting, and dielectric-process analysis of the film.

Analysis of open-circuit potential

Figure 11a presents the variation in the open-circuit potential (OCP) of each system during exposure, together with the time-integrated average value ⟨OCP⟩ (Fig. 11b). Similar to the treatment of $|Z|_{0.01\ Hz}$ in the previous section, the time-integrated average open-circuit potential over a given time interval is defined as

$$\langle OCP\rangle_{t_1-t_2} = \frac{1}{t_2 - t_1}\int_{t_1}^{t_2} OCP\ dt, \tag{4}$$

where t_1 and t_2 are the starting and ending times of the selected interval, respectively. Figure 11b shows the average OCP values for two stages, 0–12 h and 1–7 d, which are used to compare the interfacial potential state at different concentrations during the early and middle-to-late stages.

The OCP of carbon steel in a neutral NaCl solution is approximately –0.69 V, whereas in the present study, the OCP values of all groups are generally in a range of about –0.24 to –0.61 V, which are obviously more positive. This indicates that the strongly alkaline environment has established a passive state on the steel surface, consistent with the passivation mechanism described in the Section 'Passive-film

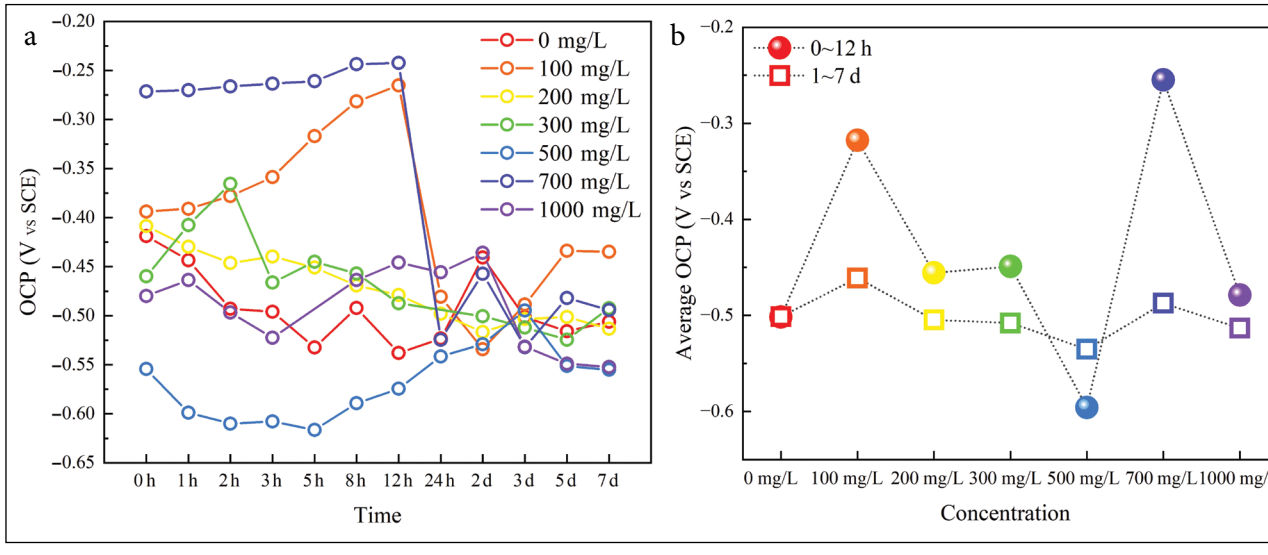

Fig. 11. (a) Open-circuit potential and (b) average open-circuit potential within 7 d for carbon steel electrodes exposed from 0 h to 5 d in 3.5 wt% NaCl + saturated $Ca(OH)_2$ solution (pH = 13.5) containing different concentrations of Xanthium extract

mechanism in alkaline environments' for alkaline simulated concrete pore solutions. As shown in Fig. 11a, the 100 and 700 mg/L groups exhibit the most pronounced positive shifts during 0–12 h, with the 700 mg/L group remaining the most positive throughout and the 100 mg/L group ranking second. This indicates that these two concentrations are the most favourable for reducing the activation degree of the steel surface at the early stage, suggesting that the adsorbed molecules can rapidly cover active sites and suppress anodic iron dissolution without excessively disrupting the initial passivation process. The 300 mg/L group also shows a certain degree of positive shift, but with larger fluctuations. The 200 mg/L group is only slightly more positive than the blank group overall. The 500 mg/L group remains the most negative throughout, indicating that this concentration is the least effective in improving the interfacial activation state. The 1000 mg/L group is not particularly prominent at the initial stage and remains only at an intermediate level.

It is noteworthy that after 24 h, the OCP values of all groups clearly converge toward a range of –0.48 to –0.53 V, and the time-integrated average OCP values for the 1–7 d stage in Fig. 11b also clearly reflect this trend. This indicates that under the continuous action of Cl^-, the differences between the initial adsorption state and the initial passivation state are gradually weakened by interfacial rearrangement, and the system enters a new mixed-potential equilibrium. This convergence is consistent with the EIS results discussed above, namely, that many concentration groups undergo film reconstruction, defect evolution, or a transition in response mechanism around 24 h. Figure 11b further shows that during the 0–12 h stage, the order of the average OCP values is approximately 700 mg/L > 100 mg/L > 300 mg/L ≈ 200 mg/L > 1000 mg/L > 0 mg/L > 500 mg/L, whereas during the 1–7 d stage, the order becomes 100 mg/L > 700 mg/L > 0 mg/L ≈ 200 mg/L ≈ 300 mg/L > 1000 mg/L > 500 mg/L. These results indicate that 700 mg/L is most favourable for promoting an early positive shift in potential, followed by 100 mg/L; during the 1–7 d stage, 100 mg/L shows the most pronounced positive average potential, while 700 mg/L still maintains a relatively good level, and 500 mg/L remains the least favourable in both stages.

However, it must be emphasised that OCP is essentially a mixed potential jointly determined by anodic dissolution and cathodic reactions, and can only reflect the thermodynamic activation tendency of the interface; it cannot be used alone as a criterion for judging inhibition performance. Therefore, although 100 mg/L shows the highest average OCP, the EIS results above indicate that its advantage is mainly concentrated in the early stage, while the impedance and reaction resistance decrease significantly at later stages. In contrast, although the average OCP of 700 mg/L is slightly lower than that of 100 mg/L, its overall impedance, Faradaic resistance and total resistance are higher, indicating that it suppresses the actual corrosion process more stably and comprehensively. The OCP of 1000 mg/L is not particularly positive, but its EIS performance is relatively good, indicating that at high concentration, the adsorbed layer, on the one hand, competes with OH^- and H_2O for interfacial sites and thus restricts the early growth of the passive film, while, on the other hand, more effectively suppresses subsequent defect propagation and film dissolution. Therefore, its protective effect cannot be judged solely by the magnitude of OCP. In contrast, the 500 mg/L group exhibits the most negative average OCP, and its film barrier performance and overall impedance are also relatively weak in the EIS analysis, indicating that no effective synergy is established between the adsorbed layer and the passive film at this concentration.

The OCP results indicate that the Xanthium inhibitor exerts a pronounced concentration-dependent effect on the activation state of the steel interface. Among the investigated concentrations, 700 mg/L is more favourable for the early positive shift in potential, whereas 100 mg/L shows a more positive average potential at the middle and later stages, while 500 mg/L is the least favourable in both stages. However, when considered together with the EIS results, 700 mg/L is the concentration that combines a relatively favourable potential state, stronger interfacial stability, and the best overall protective performance.

Analysis of polarization curves

Figure 12 show the potentiodynamic polarisation results of carbon steel after the exposure for 5 h and 7 d in solutions containing different concentrations of Xanthium extract, including the polarisation curves, corrosion potential E_{corr} (Fig. 13), corrosion current i_{corr} (Fig. 14) and polarisation resistance R_p (Fig. 14). The corrosion current density was obtained by Tafel

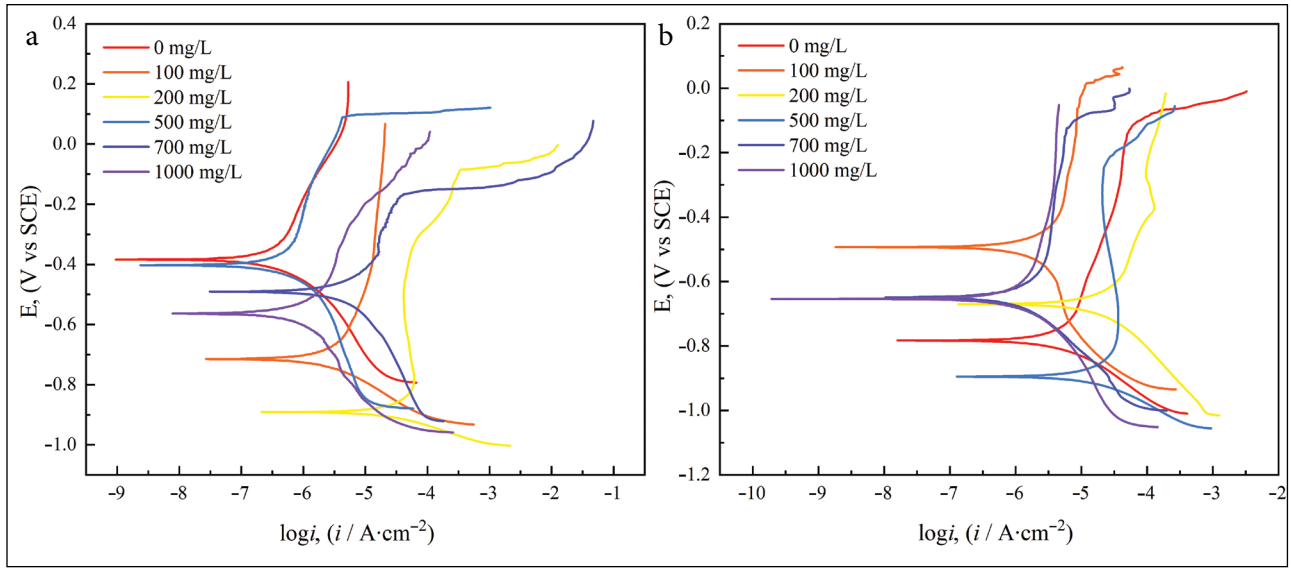

Fig. 12. Potentiodynamic polarisation curves of carbon steel electrodes exposed for (a) 5 h and (b) 7 d in 3.5 wt% NaCl + saturated $Ca(OH)_2$ solution (pH = 13.5) containing different concentrations of Xanthium extract

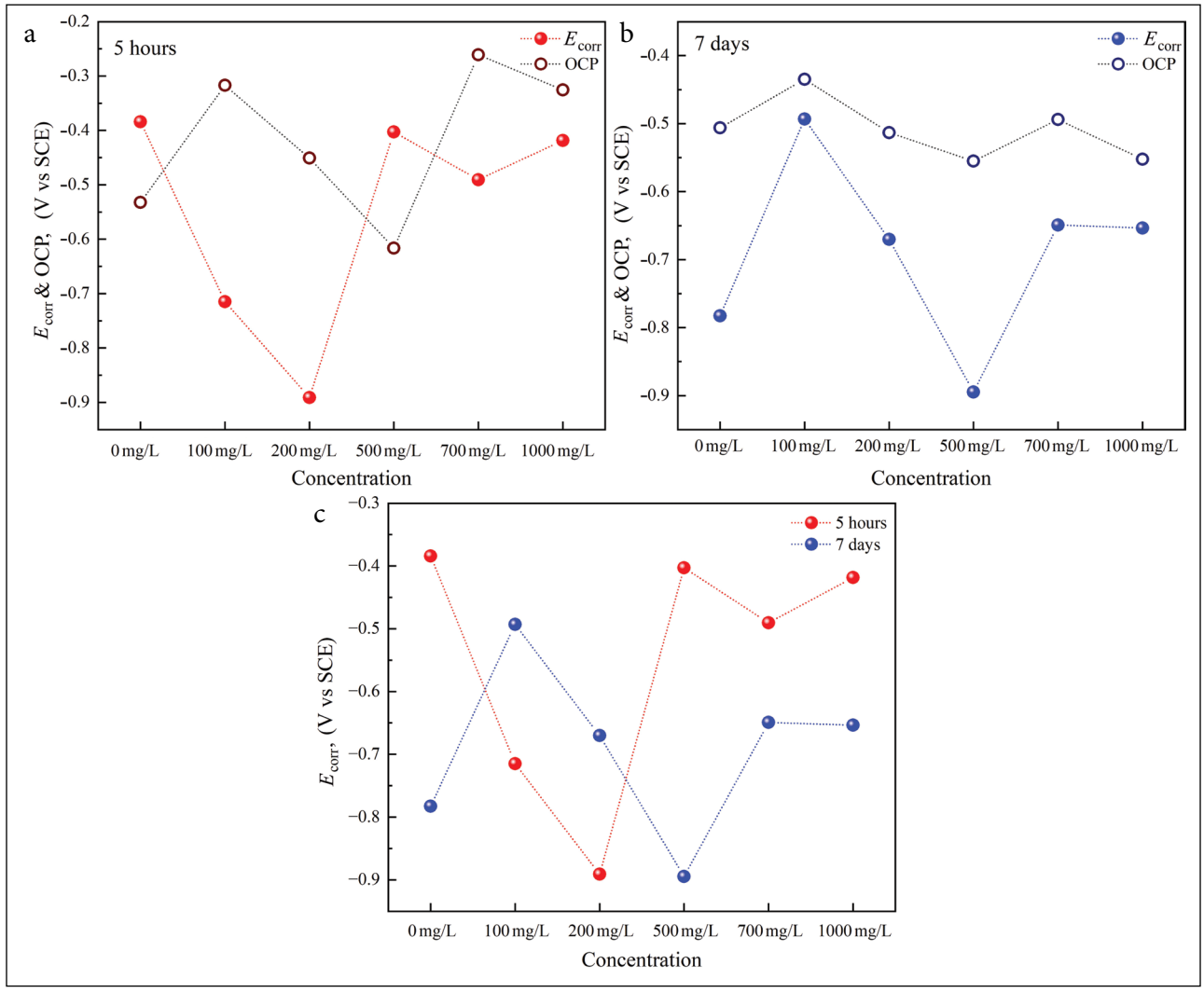

Fig. 13. Comparison of corrosion potential E_{corr} and OCP of carbon steel electrodes exposed for (a) 5 h and (b) 7 d, and (c) comparison of E_{corr} at 5 h and 7 d, in 3.5 wt% NaCl + saturated $Ca(OH)_2$ solution (pH = 13.5) containing different concentrations of Xanthium extract

fitting in the near-E_{corr} region rather than by using the whole polarisation branch [31]. The polarisation resistance was calculated using the Stern–Geary equation

$$R_p = \frac{\beta_a \beta_c}{2.303\, i_{corr} (\beta_a + \beta_c)}, \quad (5)$$

where β_a and β_c are the anodic and cathodic Tafel slopes, respectively. Therefore, both i_{corr} and R_p reflect corrosion kinetics, but they are not required to vary in complete synchrony: i_{corr} more directly represents the instantaneous corrosion current, whereas R_p is additionally affected by the anodic and cathodic polarisation slopes.

As shown in Fig. 13, clear differences exist between E_{corr} and OCP at both 5 h and 7 d. It should be noted that in this study the polarisation measurements were performed by scanning from the low-potential region of strong cathodic polarisation toward the anodic direction. The rapid oxygen reduction and other reduction processes occurring at the initial stage can impose a dynamic disturbance on the adsorption layer and passive film formed under static conditions, thereby weakening the interfacial equilibrium corresponding to OCP. Therefore, E_{corr} should not be regarded simply as a repetition of OCP, but rather as the corrosion mixed potential re-established under continuous external polarization disturbance. At 5 h, the direction and magnitude of the deviation between E_{corr} and OCP vary significantly among different concentrations, indicating that the composite film is still relatively sensitive at the early stage. At 7 d, all E_{corr} values become markedly more negative than the corresponding OCP values, indicating that after longer immersion, although the adsorption layer and passive film can maintain a certain equilibrium under open-circuit conditions, this equilibrium can still be readily disrupted under a strong cathodic prepolarisation and subsequent scanning.

At 5 h, the 200 mg/L group shows the worst polarisation performance, with the most negative E_{corr} (Fig. 13), the highest i_{corr} and the lowest R_p (Fig. 14). This indicates that at this concentration, the disruptive effect of the adsorbed molecules on the passive film is stronger than their stabilising effect, they neither form an effective coverage nor suppress the defect evolution and metal dissolution induced by Cl^-. By contrast, the blank group exhibits a relatively low i_{corr} and a relatively high R_p at 5 h, indicating that the initial passive film formed solely by the strongly alkaline environment still possesses a strong protective capability over a short period. The 1000 mg/L group also shows a relatively low i_{corr} and a relatively high R_p at 5 h, indicating that the high-concentration inhibitor has already established a strong adsorption-shielding effect. The 500 mg/L group also shows a relatively high R_p at 5 h, but this does not imply a stable subsequent protection. Combined with the EIS results above, this concentration gradually develops a restricted transport behaviour during later exposure,

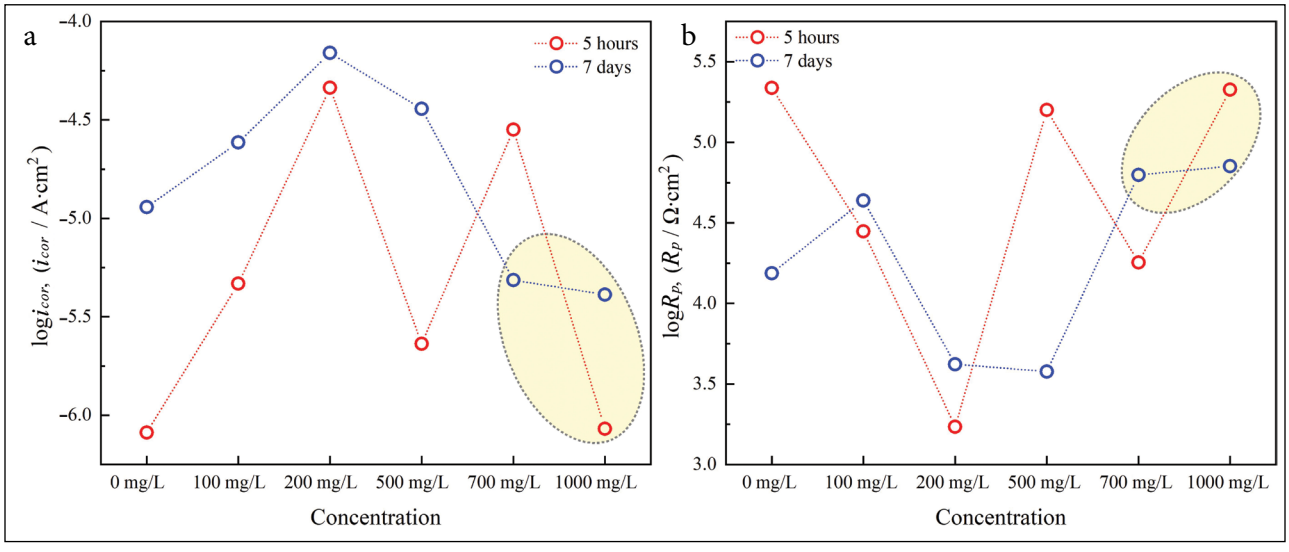

Fig. 14. (a) Corrosion current i_{corr} and (b) polarisation resistance R_p of carbon steel electrodes exposed for 5 h and 7 d in 3.5 wt% NaCl + saturated $Ca(OH)_2$ solution (pH = 13.5) containing different concentrations of Xanthium extract

indicating that its early polarisation result reflects only a temporarily high resistance under instantaneous perturbation conditions rather than a stable and durable interfacial protection. In contrast, although the 100 and 700 mg/L groups exhibit more positive OCP values and a higher overall impedance in the EIS results at 5 h, their i_{corr} and R_p do not reach the optimum values, indicating that the adsorption–passivation synergistic layers established at the early stage in these two groups are more favourable under static or weakly perturbed conditions, but are more prone to rearrangement or local weakening under a strong cathodic prepolarisation.

At 7 d, the ranking of the polarisation results becomes more clearly differentiated. The 700 and 1000 mg/L groups exhibit the lowest i_{corr} and the highest R_p (Fig. 13), indicating that these two concentrations are the most effective in suppressing actual corrosion reactions after long-term exposure. Although the difference between 700 and 1000 mg/L is no longer large, 700 mg/L still agrees better with the optimum synergistic state revealed by the EIS results, namely, a high overall impedance, a high Faradaic resistance, and the absence of a pronounced diffusion tail. The 100 mg/L group ranks next, indicating that it possesses a certain long-term inhibition capability, although less stable than that of 700 and 1000 mg/L. For the blank group, i_{corr} increases significantly and R_p decreases markedly at 7 d, indicating that the naturally formed passive film has become clearly destabilised under the continuous action of Cl^-, which is consistent with the previous analysis of the decline in the late-stage impedance and the continuous accumulation of film defects in the blank system. The 500 mg/L group exhibits the most negative E_{corr} (Fig. 13) and a very low R_p at 7 d, indicating that at this concentration the interface not only fails to form a stable composite film, but also tends to develop into a deteriorated state characterised by the coexistence of defect-dominated behaviour and restricted transport; this is fully consistent with the W_s feature observed in the EIS results after 5 h. The 200 mg/L group still maintains the highest i_{corr} and the lowest R_p, further confirming that it is the most unfavourable concentration.

Taken together, Figs 12–14 indicate that the conclusions drawn from the polarisation curves are generally consistent with those obtained from the OCP and EIS analyses, but they also reveal an important feature: a more positive OCP or a higher early-stage impedance under static conditions does not necessarily correspond directly to the lowest instantaneous corrosion current under a strong polarisation perturbation. The fundamental reason is that polarisation testing actively disrupts the original interfacial equilibrium and forces the adsorption film and passive film to respond again under dynamic scanning. Overall, the 700 mg/L group exhibits the best comprehensive polarisation performance after long-term exposure, followed by the 1000 mg/L group. The 100 mg/L group shows a certain inhibition effect, but is more characteristic of early-stage or intermediate-level protection. The 500 and 200 mg/L groups are clearly unfavourable, especially the 200 mg/L group, which shows the worst performance in all polarisation parameters. These results indicate that the effective action of the Xanthium inhibitor does not simply arise from increasing film thickness, but rather from stabilising the film structure, suppressing interfacial charge transfer, and reducing the sustained corrosion current through the synergy between the adsorption layer and the passive film at a suitable concentration. Under the present conditions, 700 mg/L is the most appropriate concentration range.

CONCLUSIONS

In this study, Xanthium extract was used as a natural corrosion inhibitor for steel rebar in a chloride-containing alkaline environment, and its influence on the interfacial behaviour of carbon steel electrodes was systematically investigated. The results show that, in saturated $Ca(OH)_2$ + 3.5 wt% NaCl solution (pH 13.5), a passive film first forms on the steel surface, and the molecules in the Xanthium extract further participate in interfacial regulation through surface adsorption. Their effect is not simply to promote film thickening, but rather to determine the protective performance jointly by influencing the integrity of the composite film structure, defect evolution, and interfacial electrochemical reactions. Clear differences are observed among different concentrations. The 100 mg/L group shows a relatively obvious early-stage positive shift in potential and an initial inhibitory effect, but its stability at the middle and later stages is limited. The 200 mg/L group exhibits the lowest overall

impedance, film resistance, and Faradaic resistance, and also gives the worst polarisation performance, making it the most unfavourable concentration. The 300 mg/L group shows obvious fluctuations in the interfacial state. The 500 mg/L group develops pronounced restricted transport characteristics at the middle and later stages and shows a relatively weak protection. The 700 mg/L group exhibits the best performance in terms of overall impedance, Faradaic resistance, total electrode-process resistance, and long-term polarisation behaviour, indicating that the best synergy between the adsorption film and the passive film is achieved at this concentration. The 1000 mg/L group also shows a good sustained protection, but its overall performance is still slightly inferior to that of the 700 mg/L group. Taken together, the OCP, EIS and polarisation results indicate that the effective action of the Xanthium inhibitor arises from the synergistic regulation of 'stabilising the interface through adsorption' and 'suppressing passive-film defect evolution', and 700 mg/L is the optimum concentration under the conditions of this study. However, the saturated $Ca(OH)_2$ + NaCl solution used in this study is only a simplified simulated concrete pore solution and does not fully reproduce the physical and chemical complexity of real concrete, such as pore structure, local pH variation, and interactions between solid hydration products and inhibitor molecules. Therefore, further verification in mortar or concrete systems is still needed.

ACKNOWLEDGEMENTS

This work has been funded by National Natural Science Foundation of China, Grand No. 51971192, Taishan Scholar Project of Shandong Province, Grand No. TSQN202306160, Natural Science Foundation of Shandong Province, Grand No. ZR2020QB071, National College Students Innovation and Entrepreneurship Training Program of the Ministry of Education of China, Grand No. 202511066004, 202511066007, and Graduate Student Science and Technology Innovation Fund of Yantai University, Grand No. KGIFYTU2517.

Received 5 March 2026
Accepted 18 June 2026

References

1. M. Ali, M. A. Shams, N. Bheel, et al., *RSC Adv.*, **14(50)**, 37252 (2024).
2. Y. Tian, G. Zhang, H. Ye, et al., *Constr. Build. Mater.*, **369**, 130504 (2023).
3. F. Bolzoni, A. Brenna, M. Ormellese, *Cem. Concr. Res.*, **154**, 106719 (2022).
4. H. Zheng, C. S. Poon, W. Li, *Cem. Concr. Compos.*, **112**, 103661 (2020).
5. R. Ding, X.-Q. Zhang, Q.-X. Yue, J. Lv, J. Liu, *Corros. Rev.*, **42(6)**, 743 (2024).
6. R. Ding, X.-Q. Zhang, X. Liang, J. Liu, *J. Build. Eng.*, **85**, 108770 (2024).
7. A. Zomorodian, A. Behnood, *Buildings*, **13(5)**, 1170 (2023).
8. X. Wang, J. Liu, M. Jin, Y. Yan, J. Tang, Z. Jin, *Constr. Build. Mater.*, **433**, 136583 (2024).
9. Z. Liu, W. Zhang, D. Zhang, J. Ouyang, Z. Wang, Y. Chen, *Case Stud. Constr. Mater.*, **21**, e04031 (2024).
10. L. Casanova, F. Ceriani, E. Messinese, et al., *Materials*, **16(23)**, 7462 (2023).
11. P. Wang, Y. Wang, T. Zhao, et al., *J. Adv. Concr. Technol.*, **18(3)**, 116 (2020).
12. Y. Bellal, F. Benghanem, S. Keraghel, *J. Mol. Struct.*, **1225**, 129257 (2021).
13. R. Naderi, A. Bautista, F. Velasco, M. Soleimani, M. Pourfath, *J. Build. Eng.*, **58**, 105055 (2022).
14. K. Subbiah, H.-S. Lee, M. R. Al-Hadeethi, T. Park, H. Lgaz, *Chem. Eng. J. (Lausanne)*, **458**, 141347 (2023).
15. A. Ghazaee, S. Pour-Ali, S. Mahdavi, R. Tavangar, M. Khalili, *Inorg. Chem. Commun.*, **167**, 112832 (2024).
16. Y. Meng, S. Li, Z. Zhang, *Heliyon*, **10(3)** (2024).
17. C. Liu, Y. Liu, Z. Xia, Z. Wang, B. Wu, *J. Build. Eng.*, **82**, 108194 (2024).
18. T. Han, H.-L. Li, Y. Hu, et al., *Zhong xi yi jie he xue bao = J. Chin. Integr. Med.*, **4(2)**, 194 (2006).
19. B. Chen, L. Ma, X. Wang, Y. Shen, X. Jia, *Pharmacogn. Mag.*, **9(34)**, 103 (2013).
20. S.-R. Yoo, C.-S. Seo, N.-R. Lee, H.-K. Shin, S.-J. Jeong, *Pharmacogn. Mag.*, **11(Suppl 4)**, S585 (2015).
21. H. Jiang, L. Yang, X. Xing, et al., *Molecules*, **23(2)**, 243 (2018).
22. H. Jiang, L. Yang, X. Xing, et al., *Phytomedicine*, **57**, 191 (2019).
23. H. Jiang, X.-J. Wang, L. Yang, et al., *World J. Tradit. Chin. Med.*, **6(4)**, 408 (2020).
24. J. Wang, D. Wang, B. Wu, J. Han, N. Tan, *Phytochem. Rev.*, **24(1)**, 773 (2025).
25. Y. Tian, J. Bao, D. Xie, et al., *J. Build. Eng.*, **65**, 105762 (2023).
26. Y. Tian, W. Guo, W. Wang, B. Wang, P. Zhang, T. Zhao, *Constr. Build. Mater.*, **368**, 130385 (2023).

27. A. K. Tiwari, P. Dogra, S. Goyal, V. Luxami, *Corros. Eng. Sci. Technol.*, **59(6)**, 381 (2024).
28. S. Joiret, M. Keddam, X. R. Nóvoa, M. Pérez, C. Rangel, H. Takenouti, *Cem. Concr. Compos.*, **24(1)**, 7 (2002).
29. D. D. Macdonald, *J. Electrochem. Soc.*, **139(12)**, 3434 (1992).
30. H.-W. Tian, W.-H. Li, D.-P. Wang, B.-R. Hou, *Acta Phys. Chim. Sin.*, **28(1)**, 137 (2012).
31. T. K. Ratajczyk, H. Cesiulis, N. Tsyntsaru, M. Donten, *Electrochim. Acta*, **556**, 148420 (2026).

Yu-chen Zhang, Xiao Liu, An-lan Ji, Rui Ding, Yi-wen Zhang, Hao-han Cao, Bing Bai, Xin-ting Ding, Rui-qin Xu, Jin-ying Li, Jie Liu

PLIENINĖS ARMATŪROS KOROZINIO ELGESIO CHLORIDŲ TURINČIOJE ŠARMINĖJE APLINKOJE ELEKTROCHEMINIS TYRIMAS IR KSANTIO EKSTRAKTO PASYVIOSIOS PLĖVELĖS ĮTAKOS MECHANIZMAS